Background

The deposition of amyloid Aβ-peptide (Aβ) in the human brain and the formation of neurofibrillary tangles (NFTs) are histopathological hallmarks of Alzheimer's disease (AD) [1,2]. Neuron loss, neuritic and synaptic degeneration are seen in addition to Aβ-plaque deposition and NFT formation and are assumed to represent the morphological correlative of cognitive decline [3-5].

Aβ is a proteolytic fragment derived from the amyloid precursor protein (APP) by β- and γ-secretase cleavage [6,7]. Aβ is the major component of extracellular senile plaques in the AD brain [2] and it has been considered to play a central role in AD pathogenesis [8]. In addition to extracellular Aβ-deposition, intracellular Aβ occurs in nerve cells in the AD brain [9,10] and in mouse models for AD [11-13]. The role of intracellular Aβ in neurodegeneration and the development of AD is discussed controversially. Mutant intracellular Aβ has been shown to induce hippocampal cell loss associated with endoplasmic reticulum stress and mitochondrial alterations in cell culture [14]. Memory impairment in APP-transgenic mice has been observed even after reduction of plaques. In these animals increased levels of intraneuronal Aβ were reported [15]. The new APP48 mouse model expresses a proenkephalin signal peptide (SPENK)-human wild type $A\beta_{42}$ construct in neurons of the central nervous system (CNS), exhibits intracellular Aβ-aggregates in neurons in the absence of Aβ-plaques, and develops CA1 neuron loss and motor deficits [16]. The name APP48 mouse is misleading because Aβ is produced independent from APP in these mice but we used the name APP48 mouse here because this mouse model was already introduced to the scientific community with this name [16]. Although Aβ production in APP48 mice differs from APP-derived Aβ production and does not model AD, APP48 mice allow the analysis of intracellular Aβ toxicity independent of APP under artificial conditions. The APP23 mouse is an Aβ-plaque producing mouse model, which overexpresses human APP with the Swedish mutation (KM670/671NL) in CNS neurons. It exhibits dendrite degeneration, loss of CA1 neurons and of asymmetric synapses in the frontocentral cortex [17-19]. In this mouse model Aβ is generated by proteolytic processing of APP by β- and γ-secretases. It accumulates extracellularly in Aβ plaques and in intracellular aggregates [13,20]. Together, these mouse models offer the possibility to compare the effect of Aβ placed into the endoplasmic reticulum and the Golgi apparatus in APP48 mice with Aβ cleaved from APP in a post-Golgi compartment [21,22] in APP23 mice. Both mice have been demonstrated to express high amounts of the transgene mRNA in neurons of the neocortex and hippocampus in a similar distribution pattern [16,20] providing comparable transgene expression levels in the respective neurons of these mouse models. Here, we investigated 1) any pathological abnormalities associated with APP-independent intracellular Aβ accumulation in APP48 mice and 2) whether APP and Aβ production by β- and γ-secretase is critical for neurodegeneration in APP23 mice rather than the mere presence of the Aβ peptide as in APP48 mice.

To address these objectives we studied dendritic morphology of frontocentral layer III pyramidal cells and synapse densities in the frontocentral cortex and the hippocampal sector CA1 of APP48 mice in comparison with APP23 and wild type mice. We determined the numbers of neurons in the frontocentral cortex as well as in the hippocampal sector CA1, and compared ultrastructural changes in neurons of APP23, APP48, and wild type mice.

Methods

Animals

APP48 mice were generated as described previously [16] and continuously back-crossed to C57BL/6. A murine Thy-1 expression cassette was used encoding the rat proenkephalin signal sequence followed by human wild type $A\beta_{1-42}$ to drive neuron-specific expression of human wild type $A\beta_{1-42}$. APP23 mice were generated as described previously [20] and continuously back-crossed to C57BL/6. The same murine Thy-1 cassette was used to drive neuron-specific expression of human APP751 with the Swedish double mutation 670/671 KM → NL. Heterozygous female APP23 mice (3 months, n = 12; 15 months, n = 17) and female and male APP48 mice (3 months, n = 12; 18 months, n = 17) were analyzed. As control, respective female and male wild type littermates of 3 (n = 14), 15 (n = 10), and 18 months (n = 10) were used.

Animals were treated in agreement with the German and Swiss laws for the use of laboratory animals.

Tissue preparation and DiI tracing

For DiI tracing the brains of 3 and 18-months-old APP48, 3 and 15-month-old APP23, and of 3 and 15-18-month-old wild type mice were studied. Mice were anesthetized. Perfusion was performed transcardially with Tris-buffered saline (TBS) with heparin (pH 7.4) followed by the injection of 0.1 M PBS (pH 7.4) containing 2.6% paraformaldehyde (PFA), 0.8% iodoacetic acid, 0.8% sodium periodate and 0.1 M D-L lysine. The brains were removed in total and post-fixed in 2.6% phosphate-buffered PFA (pH 7.4) containing 0.8% iodoacetic acid, 0.8% sodium periodate and 0.1 M D-L lysine [23]. Three days later a single crystal (0.3 mm^3) of the carbocyanine dye DiI (Molecular Probes, Eugene, OR, USA) was implanted into the left frontocentral cortex, 1 mm rostrally from the central sulcus, 2 mm laterally from the middle

line and 1 mm deep in the cortex as reported earlier [18]. This dye allows precise Golgi-like tracing of neurons in post-mortem fixed tissue in a quality similar to in vivo tracing methods [18]. After incubation in 2.6% phosphate-buffered PFA for at least 3 months at 37°C, 100 μm thick coronal vibratome sections were cut. All sections of a given mouse brain were separately stored and continuously numbered. Sections were temporarily mounted in TBS for microscopic analysis.

Microscopic and quantitative analysis

In layer III of the frontocentral cortex of the right hemisphere, contralateral to the implantation site of the tracer, the morphology of traced commissural neurons was examined. The traced neurons were assigned to different types according to their morphology [18] (Additional file 1). Then the number of traced commissural neurons of each type in wild type mice was counted and compared with that in APP23 and APP48 mice. For qualitative and quantitative analysis 10 consecutive sections (100-μm thickness each) representing a tissue block of 1 mm thickness were studied for each mouse. Analysis started at the anterior commissure setting the caudal limit of the investigated tissue block. For each coronal section, the medial boundary of the region investigated was set as the vertical line at the cingulum that separated the cingulate cortex from secondary motor cortex (M2). The horizontal boundary was set as the horizontal line separating the primary somatosensory cortex (S1) from the insular cortex.

For the qualitative analysis a laser scanning confocal microscope (Leica TCS NT, Leica, Bensheim, Germany) was used. Stacks of 2D images were superimposed digitally using the Image J Image Processing and Analysis software (NIH, Bethesda, MD, USA), and 3D data sets were generated for the visualization of neurons with their entire dendritic tree. For quantification, traced neurons in layer III were counted in the region of interest in 10 consecutive sections of the tissue block taken for qualitative and quantitative analysis using a fluorescence microscope (Leica DMLB, Leica). In so doing, we analyzed a cortex volume of 5–6 mm^3 in each mouse. Mean and median values of the number of traced neurons were calculated and compared between wild type, APP23, and APP48 mice.

Immunohistochemistry

Immunohistochemistry was performed for the visualization of Aβ pathology as well as dendritic morphology in APP48 and APP23 mice. After formic acid pretreatment free-floating sections were incubated in goat anti-mouse immunoglobulin (IgG) to block cross-reactions with intrinsic mouse IgG as previously described [24]. To detect Aβ-positive material the sections were stained with monoclonal antibodies specifically detecting the C-terminus of $Aβ_{42}$ (MBC42 [25], 1/200). In APP23 mice anti-$Aβ_{17-24}$ (4G8; 1/5000, Sigma-Aldrich, St. Louis, USA) was used to stain Aβ-deposits regardless of the $Aβ_{40}$ or $Aβ_{42}$ C-terminus. MBC40 ([25], 1/20) antibodies detecting exclusively the C-terminus of $Aβ_{40}$ were used in APP23 mice as well. N-terminal-truncated and pyroglutamate modified $Aβ_{N3pE}$ was detected with anti-$Aβ_{N3pE}$ (polyclonal rabbit, 1/100, additional microwave pretreatment, IBL International GmbH, Hamburg, Germany [26]). Phosphorylation of serine 8 of Aβ was detected with antibodies against phosphorylated Aβ (pAβ; SA5434, 1/5; 1E4E11, 1/50, additional microwave pretreatment [27,28]). The primary antibodies were detected with a biotinylated secondary antibody and the ABC complex (Vectastain, Vector laboratories (Burlingame, CA. USA)), and visualized with DAB [29]. Sections were mounted in Eukitt© (Kindler, Freiburg, Germany). The immunostained sections were analyzed with a Leica DMLB fluorescence microscope (Leica, Bensheim, Germany). Positive and negative controls were performed.

Protein extraction from brain tissue

Protein extraction was carried out from female APP23 (n = 4), APP48 (n = 4), and wild type littermates (n = 4) mouse brains, aged 9–11 months. Mice of this age were taken to demonstrate the differences in the biochemical distribution of Aβ in APP23 and APP48 mice.

Fresh frozen forebrain (0.4 g) was homogenized in 2 ml of 0.32 M sucrose dissolved in Tris-buffered saline (TBS) containing a protease and phosphatase inhibitor-cocktail (Complete and PhosphoSTOP, Roche, Mannheim, Germany) with Micropestle (Eppendorf, Hamburg, Germany) followed by sonication. The homogenate was centrifuged for 30 min at 14.000 × g at 4°C. The supernatant (S1) with the soluble and dispersible fraction not separated from one another was kept. The pellet (P1) containing the membrane-associated and the insoluble, plaque-associated fraction was resuspended in 2% SDS.

Ultracentrifugation of the supernatant S1 at 175.000 × g was used to separate the soluble, i.e. the supernatant after ultracentrifugation (S2), from the dispersible fraction, i.e. the resulting pellet (P2). The pellet P2 with the dispersible fraction was resuspended in TBS.

The SDS-resuspended pellet P1 was centrifuged at 14.000 × g. The supernatant (S3) was kept as membrane-associated SDS-soluble fraction. The pellet (P3) that remained was dissolved in 70% formic acid and dried in a vacuum centrifuge (Vacufuge, Eppendorf, Hamburg, Germany) and reconstituted in 100 μl of 2X LDS (lithium dodecyl sulfate) sample buffer (Invitrogen, Carlsbad, CA, USA) followed by heating at 70°C for 5 min. The resultant sample was considered as insoluble, plaque-associated fraction [30]. The total protein amounts of soluble, dispersible, and membrane-associated fractions

were determined using BCA Protein Assay (Bio-Rad, Hercules, CA, USA).

SDS-PAGE and western blot analysis

For SDS-PAGE, soluble (S2), dispersible (P2), membrane-associated (SDS-soluble; S3), and insoluble, plaque-associated (formic acid soluble; P3) fractions (50 μg total protein) were electrophoretically resolved in a precast NuPAGE 4-12% Bis-Tris gel system (Invitrogen). The protein load was controlled either by Ponceau S staining or β-actin (C4, 1/1000, Santa Cruz Biotechnology, Santa Cruz, CA, USA) immunoblotting.

Aβ was detected by western blotting with anti-$A\beta_{1-17}$ (6E10, Covance, Dedham, USA, 1/1000). Blots were developed with an ECL detection system (Supersignal Pico Western system, ThermoScientific-Pierce, Waltham, MA, USA) and illuminated in ECL Hyperfilm (GE Healthcare, Buckinghamshire, UK).

Aβ ELISA

For analysis of Aβ by ELISA, forebrain homogenates from APP23 and APP48 mice of each age group (2–3 months: n = 6 (APP23), 6 (APP48); 15–18 months: n = 7 (APP23), 8 (APP48)) were homogenized, centrifuged and loaded on sandwich ELISA plates for quantification of Aβ peptides ($A\beta_{42}$: ELISA from Innogenetics, Ghent, Belgium) as previously described [18]. Standard curves were prepared with synthetic $A\beta_{1-42}$ purchased from Bachem and diluted in extracts of non-transgenic mouse forebrain prepared in parallel as described above. Each sample was analyzed in duplicate.

Stereology

Six APP23, six APP48, and six wild type mice at the ages of 3 and 15-18-months, respectively, were chosen randomly for stereology. One brain section of the frontocentral cortex already quantified for the number of DiI-traced neurons was selected by chance and stained with aldehyde fuchsin-Darrow red. Quantification of neurons was performed according to the principles of unbiased stereology [31]. The frontocentral cortex volume was defined as the volume of the subfields M2, M1, S1 starting at the level of the anterior commissure as described previously [18]. The CA1 volume was measured in serial 100 μm thick sections of the entire mouse brain at 5x magnification. Neurons were counted in three different, randomly chosen microscopic fields (40x objective magnification) of an aldehyde fuchsin - Darrow red stained section of the frontocentral cortex and CA1, respectively. For optical dissection, stacks of 10 images in 2 μm focus distance were generated for each microscopic field. Only those neurons having nuclei with dark and round nucleoli visible in the center of soma in one of the stack-images were considered for quantification using the ImageJ software (NIH, Bethesda, USA). The number of neurons in the frontocentral cortex and CA1 was calculated on the basis of the respective reference volumes and neuron densities.

Electron microscopy, immunoelectron microscopy and semiquantitative assessment of synapse densities and mitochondrial alterations

100 μm thick vibratome sections of the frontocentral cortex and of the hippocampus from six wild type, six APP23, and six APP48 mice, aged 3 and 15–18 months respectively, were flat-embedded in Epon (Fluka, Germany). A second vibratome section from each animal and region was flat embedded in LR-White-Resin (Hard-grade Acrylic Resin; London Resin Company, Berkshire, UK). A part of the frontocentral cortex covering all six cortical layers was dissected under microscopic control and pasted on Epon blocks with a drop of Epon. Likewise, a part of the CA1 subfield of the hippocampus with adjacent stratum oriens and radiatum was cut and pasted on a second Epon block ultrathin sections were cut at 70 nm. Epon sections were block stained with uranyl acetate and lead citrate, and viewed with a Philips EM400T 120KV (Philips, Eindhoven, The Netherlands), a Zeiss EM10 (Zeiss, Oberkochen, Germany), or a JEM-1400 (JEOL, Tokyo, JP) electron microscope. LR-White sections were immunostained with anti-$A\beta_{42}$ (MBC42) and anti-$A\beta_{1-17}$ (6E10, Covance, Dedham, USA, 1 mg/ml) antibodies and visualized with anti-mouse secondary antibodies (Aurion Immuno Gold Reagents & Accessories, Wageningen, The Netherlands) labeled with 10 nm nanogold particles. Digital pictures were taken.

Digital pictures from Epon embedded sections were taken from 20 soma- and plaque-free neuropil areas located in layers II-VI at 4600-times magnification. The numbers of the symmetric and asymmetric synapses were counted and the length of the synapses was determined with the ImageJ software (NIH, Bethesda, USA). The synaptic density was determined separately for symmetric and asymmetric synapses according to DeFelipe et al. [32] (synaptic density = number of synapse-profiles in a given area / length of synaptic profiles). These semiquantitative data were used to compare the synaptic densities between the different mouse lines. Asymmetric and symmetric synapses were distinguished according to published criteria [33,34].

Synaptic densities in the CA1 regions were measured in 10 randomly taken pictures of the stratum oriens and in 10 randomly taken pictures of the stratum radiatum at 4600-times magnification.

The frequency of dystrophic neurites was observed by counting the number of dystrophic neurites in the 20 pictures taken for the determination of the synapse densities. The criteria for the identification of dystrophic

neurites at the ultrastructural level were: neurite profiles with a disorganized cytoplasm, occurrence of multilamellar structures in the absence of ultrastructurally intact cell organelles in the area of the lesion, and an enlarged size compared with neighboring neuritic profiles (Figure 1) [19]. Neurites of apoptotic or necrotic neurons, which are not enlarged and do not accumulate multilamellar bodies, were not considered as dystrophic neurites. The number of such dystrophic neurites was determined in six APP23, six APP48 and six wild type mice, aged 3 and 15–18 months respectively, and used as a semiquantitative score for structural neuritic alterations.

To clarify whether APP-independent production of intraneuronal Aβ or APP-derived extra- and intracellular Aβ accumulation are critical for mitochondrial changes in neurons we compared mitochondrial alterations in frontocentral and CA1 neurons of six APP23, six APP48 and six wild type mice, aged 3 and 15–18 months respectively, at the electron-microscopic level. For this purpose we measured the area profiles from neuritic and somatic neuronal mitochondria as well as from the respective somata and peripheral neurites in plaque-free areas. Mitochondria in peripheral dendrites and axons were analyzed in the 20 pictures from soma- and plaque-free areas of the frontocentral cortex and in 20 pictures of the stratum oriens and radiatum of the CA1 hippocampal subfield also used for the assessment of synapse densities. The mitochondria in neuronal somata were studied in 40 pictures from 10 different, randomly taken, layer II - layer VI neurons of the frontocentral cortex and in 40 pictures from 10 randomly taken CA1 neurons at 6000-times magnification (4 pictures per neuron) in each individual mouse. The area profiles from morphologically intact mitochondria and from those with an altered ultrastructure, i.e. degeneration of christae as described previously in prion disease [35], were separately obtained for somatic and peripheral neuritic mitochondria. Volume densities in percent of soma and neurite profiles were calculated according to the criteria for unbiased stereology [36] following the determinations provided in Table 1. Image processing and analysis software was used (ImageJ NIH, Bethesda, MD, USA) for this purpose. Assessments were performed without previous knowledge of the genotypes of the animals.

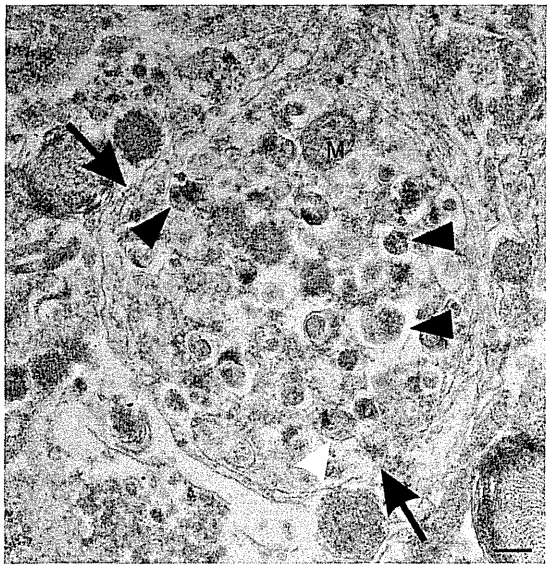

Figure 1 Identification of dystrophic neurites. Electron microscopy was used to identify dystrophic neurites (arrows) as previously described [19] and shown here in the frontocentral cortex of 15-month-old APP23 mice. Such neurites are characterized by neuritic swelling and contain vesicles with electron dense bodies (black arrowheads) probably representing autophagic vacuoles. Mitochondria in these neurites appear morphologically intact (M). Few multivesicular bodies are seen in these neurites as well (white arrowhead). The calibration bar corresponds to: 250 nm.

Statistical analysis

SPSS 19.0 (SPSS, Chicago, IL, USA) software was used to calculate statistical tests. Non-parametric tests were used to compare wild type, APP23, and APP48 mice. p-values were corrected for multiple testing using the Bonferroni method. Parametric data were analyzed by ANOVA with subsequent Games-Howell post-hoc test to correct for multiple testing or using the Welch test. The results of the statistical analysis are summarized in Additional file 2.

Results

Different patterns of Aβ-pathology in APP23 and APP48 mice

As previously published 15-month-old APP23 mice exhibited a high number of extracellular Aβ-plaques in the cerebral cortex (Figure 2a - indicated by arrows) as well as cerebral amyloid angiopathy as previously described in male and female animals [37]. Intracellular $A\beta_{42}$ detectable with MBC42 was not abundant at the light microscopic level in this region neither in neurons nor in glial cells. MBC40-positive $A\beta_{40}$ was observed in the perikarya of pyramidal neurons. At 3 months of age APP23 mice did not exhibit Aβ plaques or vascular Aβ deposits as previously described in male and female animals [37]. APP48 mice, on the other hand, did not show Aβ-plaques but intracellular accumulation of Aβ in dendritic threads, somatic granules in neurons, and in microglial Aβ-grains at 3 and 18 months of age (Figure 2b) [16]. This pathology was seen in male and female animals.

Modified Aβ such as $A\beta_{N3pE}$ was detected in a large number of plaques in 15-month-old APP23 mice (Figure 2c). In APP48 mice only few dendritic threads exhibited $A\beta_{N3pE}$ at 3 months of age (Figure 2d) whereas

Table 1 Determinations of the parameters employed for quantification of mitochondrial alterations in neurites and nerve cell somata

Percentage of altered mitochondria in nerve cell somata =	$\frac{\left(\sum \text{area of altered mitochondria within nerve cell somata}\right)}{\sum \text{area of all mitochondria within nerve cell somata}} \times 100$
Percentage of altered mitochondria in neurites (axons and dendrites) =	$\frac{\left(\sum \text{area of altered mitochondria within neurites}\right) \times 100}{\sum \text{area of all mitochondria within neurites}}$
Mitochondrial volume density in the nerve cell somata =	$\frac{\left(\sum \text{area of all mitochondria within nerve cell somata}\right) \times 100}{\sum \text{area of nerve cell somata}}$
Mitochondrial volume density in neurites =	$\frac{\left(\sum \text{area of all mitochondria within neurites}\right) \times 100}{\sum \text{area of neurites}}$
Volume density of altered mitochondria in the nerve cell somata =	$\frac{\left(\sum \text{area of altered mitochondria within nerve cell somata}\right) \times 100}{\sum \text{area of nerve cell somata}}$
Volume density of altered mitochondria in neurites =	$\frac{\left(\sum \text{area of altered mitchondria within neurites}\right) \times 100}{\sum \text{area of neurites}}$

at 18 months of age a significant number of $A\beta_{N3pE}$-positive inclusions was observed as shown previously [16]. Phosphorylated Aβ (pAβ) in APP23 mice was detected in plaques of 15 months old APP23 mice (Figure 2e). Intraneuronal pAβ in APP23 mice was apparent as previously reported in APP-PS1 transgenic animals [28]. Only single pAβ-positive threads were stained in 3-month-old APP48 mice (Figure 2f) whereas a few more pAβ-positive threads, grains and somatic granules were observed at 18 months of age.

Biochemical analysis revealed that 3-month-old APP48 mice contained ~70 times more total $A\beta_{42}$ detected by ELISA than APP23 mice whereas at 15–18 months of age APP23 mice contained $A\beta_{42}$ in a concentration ~17 fold higher than in APP48 mice (Figure 3a, Additional file 2a).

To document the distribution of Aβ aggregates we analyzed brain homogenates of 9-11-month-old APP23 and APP48 mice for Aβ in the soluble (S2), dispersible (P2), membrane-associated (S3) and insoluble fraction (P3). APP23 mice exhibited soluble, dispersible, membrane-associated and insoluble, plaque-associated Aβ (Figure 3b) as reported previously in detail [19]. In contrast, APP48 mice only exhibited dispersible, membrane-associated and insoluble, aggregated Aβ whereas soluble Aβ was not detectable (Figure 3b).

Degeneration of neurites and asymmetric synapses in APP23 but not in APP48 mice

Using retrograde tracing with DiI three types of commissural neurons were subclassified as previously published (Additional file 1) [18] in APP23, APP48, and wild type mice. Type I and type II commissural neurons exhibited alterations in the dendritic tree as well as a decrease in number in 15-month-old APP23 mice compared to wild type littermates as previously reported [18] (Figure 4a-f, Additional file 2). Type III commissural neurons did not exhibit differences in their morphological appearance among APP48, APP23, and wild type littermates (Figure 4f). There were no significant differences in the numbers of type I, II, and III commissural neurons in 3- and 18-month-old APP48 mice and in 3-month-old APP23 mice compared to the respective wild type littermates (Figure 4c-i, Additional file 2b). Thus, 15-month-old APP23 mice exhibited dendritic degeneration of frontocentral commissural neurons whereas APP48 mice did not.

To confirm neuritic degeneration we used transmission electron microscopy to compare the presence of dystrophic neurites among APP23, APP48 and wild type mice. The frequency of dystrophic neurites was higher in the frontocentral cortex of 15-month-old APP23 mice when compared to 15-18-month-old APP48 and wild type mice (Figure 5, Additional file 2c). There were no differences in the frequency of dystrophic neurites between APP48 and wild type mice or between 3-month-old animals of each genotype (Figure 5).

Qualitative changes in synapse morphology other than the generation of dystrophic neurites in 15-month-old APP23 mice were not observed. Semiquantitative analysis of the densities of symmetric and asymmetric synapses showed a reduction of the density of asymmetric synapses in the frontocentral cortex of 3 and 15-month-old APP23 mice in comparison to WT mice. In the stratum radiatum and oriens of CA1 a similar trend was observed but did not reach significance. Such a reduction of asymmetric synapses was not observed in APP48 mice in comparison to wild type littermates. Moreover, 3-month-old APP48 mice exhibited more asymmetric synapses than wild type controls (Figure 6a, Additional file 2d). There were no significant differences

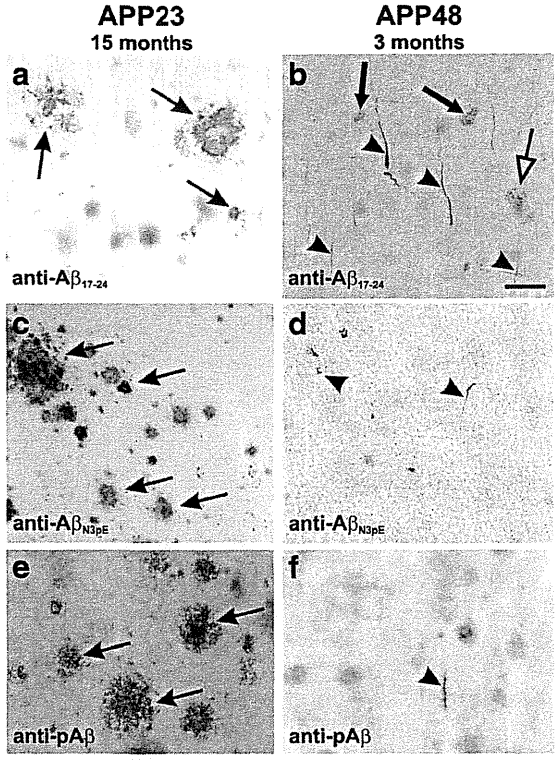

Figure 2 Aβ-pathology in 15-month-old APP23 (a, c, e) and 3-month-old-APP48 mice (b, d, f). a: The APP23 mouse showed a high number of extracellular Aβ plaques detectable with an antibody raised against $Aβ_{17-24}$ (arrows). Intracellular Aβ was negligible. **b**: In the 3-month-old APP48 mouse no extracellular Aβ-pathology was apparent. These animals showed intraneuronal dendritic threads (arrowheads) and somatic granules (lucent arrow) as well as intramicroglial Aβ-grains (arrows) detectable with anti-$Aβ_{17-24}$ as previously published [16]. **c**: Amyloid plaques in APP23 mice did also contain N-terminal truncated and pyroglutamate modified $Aβ_{N3pE}$ (arrows). **d**: $Aβ_{N3pE}$ was also found in even 3-month-old APP48 mice in some neuritic threads (arrowheads). **e**: phosphorylated Aβ (pAβ) was detected in amyloid plaques in 15-month-old APP23 mice. **f**: In 3-month-old APP48 mice only single threads showed labeling with anti-pAβ. Calibration bar in **b** corresponds to: **a, b** = 30 μm; **c** = 80 μm; **e** = 60 μm; **d, f** = 20 μm.

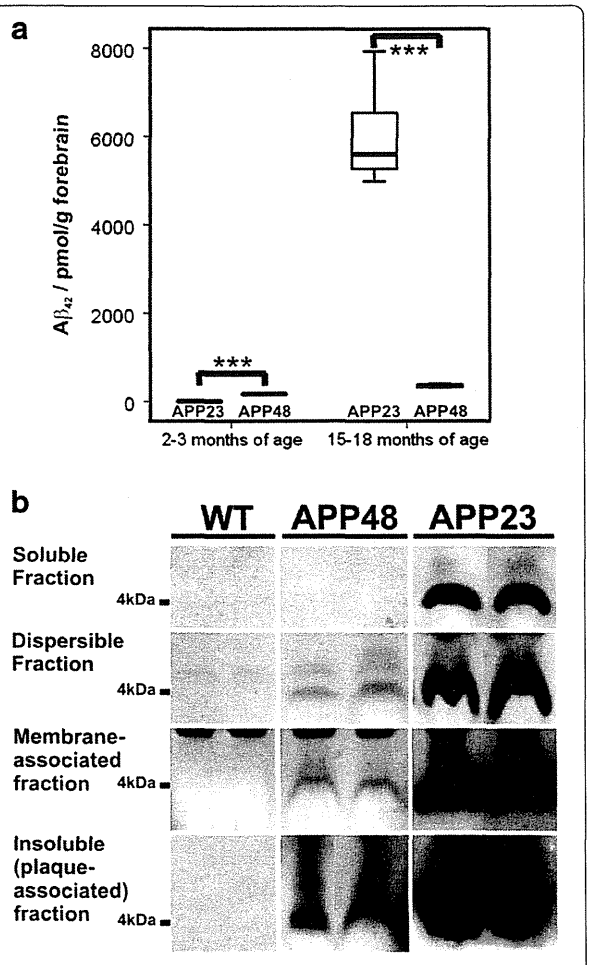

Figure 3 Biochemical analysis of Aβ in APP23 and APP48 mice. a: Total $Aβ_{42}$ levels detected by ELISA in forebrain hemispheres of 2–3 and 15-18-month-old APP23 and APP48 mice. At 2–3 months APP23 mice exhibited low amounts of $Aβ_{42}$ whereas APP48 mice displayed significantly more $Aβ_{42}$ in the brain. At 15–18 months APP48 mice showed more Aβ than at 2–3 months of age but APP23 mice exhibited several times more Aβ in the forebrain. **b**: For demonstration of the types of Aβ aggregates in APP23 and APP48 mice brain homogenates of 9-11-month-old animals were analyzed by SDS-PAGE and western blotting after preparation of the soluble, dispersible, membrane-associated and insoluble (plaque-associated) fraction. Soluble Aβ as detected with antibodies raised against $Aβ_{1-17}$ (6E10) was restricted to APP23 mice. Dispersible, membrane-associated, and insoluble (plaque-associated, formic acid soluble) Aβ aggregates were found in both transgenic mouse lines. The Aβ detected in the insoluble fraction of the forebrain homogenates of APP48 mice represents Aβ aggregates that require formic acid pretreatment before analysis similar to plaque-associated Aβ in APP23 mice. Since APP48 mice did not develop Aβ plaques this insoluble Aβ presumably represented intracellular fibrillar aggregates, such as dendritic threads. Wild type controls did not exhibit detectable amounts of Aβ in all four fractions. The original western blots are depicted in Additional file 3 (ELISA data from APP23 mice were previously published in a different context [18]). ***$p < 0.001$ Welch-test.

in the numbers of symmetric synapses among APP23, APP48, and WT mice (Figure 6b, Additional file 2d).

The number of asymmetric synapses increased with age in the frontocentral neocortex of wild type, APP23, and APP48 mice (Figure 6a, Additional file 2d). Such an increase in the number of asymmetric synapses with age was not seen in the stratum radiatum and oriens of CA1 (Figure 6a, Additional file 2d). The number of symmetric synapses did not differ between 3 and 15-18-month-old mice of each genotype (Figure 6b, Additional file 2d).

Immunoelectron microscopy showed Aβ within dendrites of 15-18-month-old APP23 and APP48 mice. In 15-month-old APP23 mice extracellular Aβ plaques contained fibrillar Aβ that could easily be labeled with

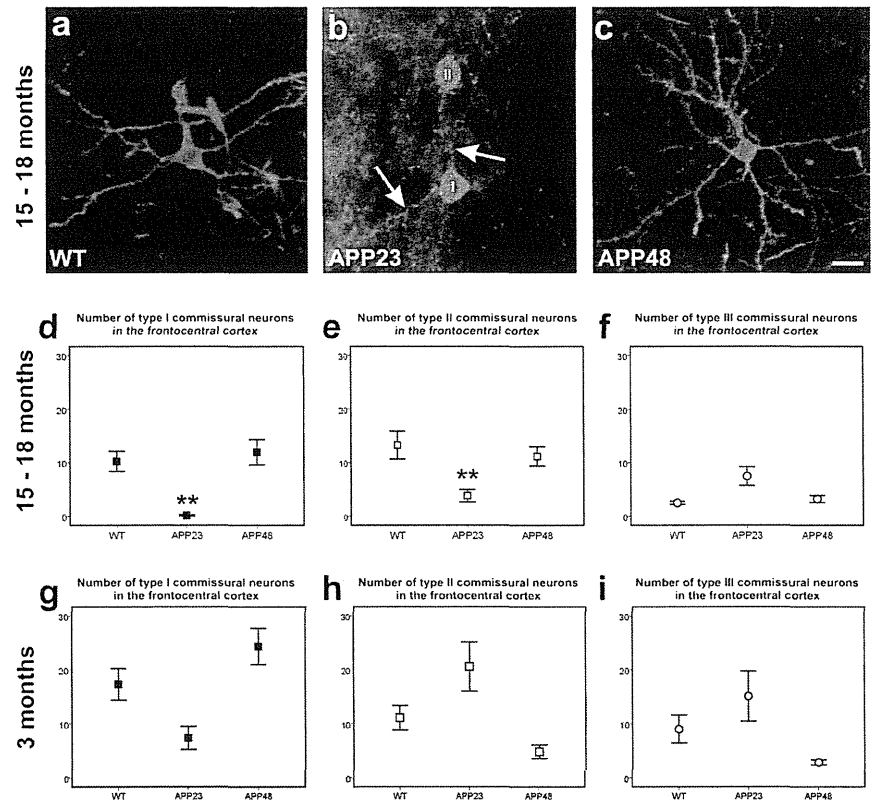

Figure 4 Dendritic degeneration in frontocentral commissural neurons of APP23 and APP48 mice. a: A type I neuron in an 18 month-old wild type animal exhibits a symmetric dendritic tree with prominent secondary and tertiary branches. **b**: In contrast, the dendritic tree of a representative type I commissural neuron (I) in a 15-month-old APP23 mouse is degenerated. Most basal dendrites were shrunken and had a reduced caliber (arrows). The degenerated dendrites showed some branches (arrows) that distinguished the degenerated type I neuron (I) from type II neurons without ramifications near the soma (II). **c**: Such a degeneration of the dendritic tree was not seen in APP48 mice. **d-f**: Numbers of DiI-traced type I, type II and type III commissural neurons in 15-18-month-old mice. **d**: APP23 mice at 15 months of age showed a decrease by more than 50% of the type I commissural neurons compared with 18-month-old wild type and APP48 mice. **e**: There was a significant reduction of type II commissural neurons in APP23 mice at 15 months of age compared with wild type littermates and APP48 mice at 18 months of age. **f**: Although APP23 mice had higher numbers of type III commissural neurons there was no significant difference from wild type littermates. **g-h**: No significant differences among the frequencies of DiI-traced type I, type II, and type III commissural neurons were observed at 3 months of age. ** $p < 0.01$ (Further statistical analysis: Additional file 2). Means and standard errors are depicted in **d-i**. (Quantitative data from APP23 mice and their respective wild type littermates were previously published in a different context [18]). Calibration bar in **c** corresponds to: **a-c** = 30 μm.

anti-$A\beta_{1-17}$ (Figure 7a, b). Plaque-associated dystrophic neurites were seen in the middle of bundles of extracellular Aβ fibrils. No fibrillar Aβ was found within neurites of APP23 mice. However, intracellular Aβ was detected in a few of these dystrophic neurites near the membrane in electron dense spherical particles, which may represent non-fibrillar Aβ oligomers or protofibrils (Figure 7c-e). In APP48 mice fibrillar Aβ aggregates presumably representing the ultrastructural correlate of dendritic threads were found in the dendrites as seen morphologically in Epon-embedded tissue. These dendrites were not enlarged (Figure 7f). Immunoelectron microscopy with anti-$A\beta_{1-17}$ indicated that the fibrillar structures identified in the Epon-embedded sections contain Aβ (Figure 7g) [16]. Organelles near dendritic threads in APP48 mice, thereby, did not differ from that elsewhere in APP48 mouse neurons as demonstrated for a mitochondrium in Figure 7g (m).

Neuron loss in the CA1 subfield but not in the frontocentral cortex of APP48 and APP23 mice

The number of CA1 neurons was lower in 3- and 18-month-old APP48 mice compared to wild type animals indicating CA1 neuron loss in APP48 mice [16]. A decrease in the number of CA1 neurons was also observed in 3- and 15-month-old APP23 mice in comparison to wild type animals (Figure 6c, Additional file 2e) [19].

In contrast, the number of neurons in the frontocentral cortex of 15-18-month-old APP23 and APP48 mice was not significantly different from that in wild type mice (Figure 6d, Additional file 2e) [16]. Therefore, we

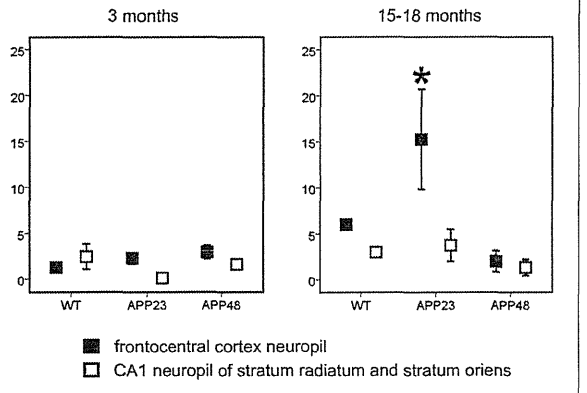

Figure 5 Frequencies of dystrophic neurites in wild type, APP23, and APP48 mice. The semiquantitatively assessed frequency of dystrophic neurites in the soma- and plaque-free frontocentral neuropil at the electron microscopic level was higher in 15-month-old APP23 mice than in wild type and APP48 mice of the same age group. In APP48 mice there was no increase in the frequency of dystrophic neurites in comparison to wild type mice. 3-month-old mice did not exhibit significant differences in the frequency of dystrophic neurites among the 3 genotypes nor were differences found in neuropil of the stratum radiatum and oriens of the CA1 region. (Data from APP23 mice and their respective wild type littermates were previously published in a different context [19]). *$p < 0.05$ (Further statistical analysis: Additional file 2). Means and standard errors are depicted.

did not analyze 3-month-old animals for the numbers of frontocentral neurons.

Increased mitochondrial alterations in neuronal somata of APP48 but not of APP23 mice

The analysis of mitochondrial alterations in neurites and the somata of frontocentral neurons showed differences between 15-18-month-old WT, APP23, and APP48 mice (Figure 8a-f). Increased percentages and volume densities of altered mitochondria exhibiting destruction and rarefaction of the christa membranes as depicted in Figure 8c were observed in somata of neurons from APP48 mice in contrast to predominantly ultrastructurally intact mitochondria in wild type and APP23 mice (Figure 8a, b, d, e, Additional file 2f,g). However, few altered mitochondria were also observed in wild type and APP23 mice. Such an increase in the percentage and volume density of altered mitochondria in APP48 mice was not observed in the hippocampal subfield CA1 and in the frontocentral neocortex of 3-month-old animals (Figure 8d, e, g, h, Additional file 2f, g). Neurites studied distant from nerve cell somata exhibited a small number of altered mitochondria in all mice but did not show differences in the percentage and volume densities of altered mitochondria among the three mouse lines at both ages and locations (Additional file 2i, j, Additional file 3a-c). The volume densities of somatic and neuritic mitochondria in general, i.e. unaltered and altered mitochondria together, did not significantly differ in APP23, APP48 and wild type mice (Figure 8f, i, Additional file 2h, k, Additional file 3c, f).

In the neuronal somata, the percentages and volume densities of altered mitochondria in frontocentral and CA1 neurons increased with age (Figure 8d, e, g, h, Additional file 2f, g). The volume densities of all, altered and healthy-looking mitochondria increased in APP23 and APP48 mice with age whereas in wild type animals such an increase was not observed (Figure 8f, i, Additional file 2h).

In neuritic processes, an increase or at least an increasing trend with age in the percentages and volume densities of altered mitochondria was observed in the frontocentral cortex of APP23, APP48 and wild type mice (Additional file 2k, Additional file 4a, b). In the stratum radiatum and oriens neurites of CA1, the percentages and volume densities of altered mitochondria in 15-month-old APP23 mice were lower than in wild type mice whereas no differences were observed between 3-month-old APP23 and wild type mice as well as between APP48 mice of any age and wild type mice (Additional file 2k, Additional file 4d, e). In neurites, the volume densities of all, healthy-looking and altered mitochondria did not increase with age (Additional file 2k, Additional file 4c, f).

At the electron microscopic level Aβ was detected in lipofuscin granules or in association with other cytoplasmic material in neurons of APP23 (Figure 7c-e, Figure 9j, k) and APP48 mice as previously reported [16,19,38] with or without mitochondrial alterations. Even neurons of wild type mice without detectable Aβ contained single altered mitochondria. In 15-month-old APP23 mice Aβ was seen only in few mitochondria (Figure 9c) whereas most somatic and neuritic mitochondria did not contain Aβ-positive material (Figure 9b). In contrast, altered and non-altered mitochondria labeled for Aβ showing gold particles in association with mitochondrial membranes were often found in the nerve cell somata of 18-month-old APP48 mice (Figure 9d, e).

Discussion

This study shows that APP-derived extra-and intracellular Aβ pathology in 15-month-old APP23 mice was associated with neuron loss, synapse loss and with neuritic alterations in non-apoptotic and non-necrotic neurons. On the other hand, APP-independent intraneuronal accumulation of Aβ in the absence of Aβ plaques in APP48 mice lead to a loss of neurons in the CA1 region [16] and to mitochondrial alterations but not to neuritic and synaptic degeneration in non-apoptotic and non-necrotic neurons. Both, extracellular plaques in APP23

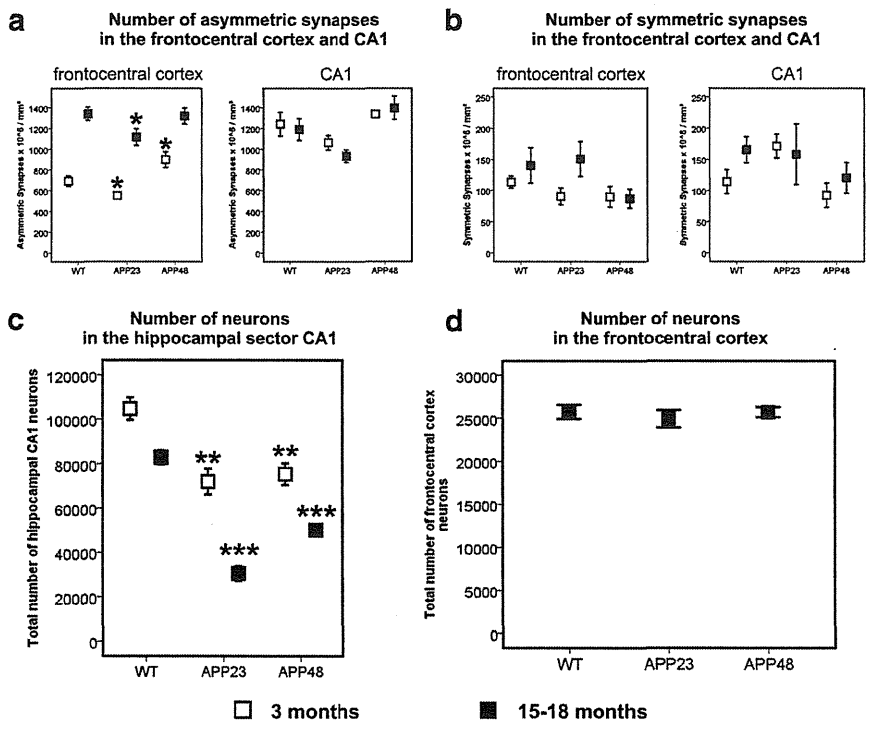

Figure 6 Synapse densities in wild type, APP23 and APP48 mice. a: Loss of asymmetric synapses in the frontocentral cortex of 3- and 15-month-old APP23 mice in comparison to wild type mice. 18-month-old APP48 and wild type mice did not differ significantly in the density of asymmetric synapses. At 3 months of age APP48 mice had even more asymmetric synapses than wild type animals. In CA1 there were also slightly less asymmetric synapses in APP23 mice than in wild type controls and APP48 mice. However, these differences were not significant. **b**: There were no significant differences in the number of symmetric synapses in the frontocentral cortex and in CA1 in 3- and 15-18-month-old animals. **c**: APP23 and APP48 mice of both age groups exhibited reduced numbers of CA1 neurons compared to wild type mice whereby CA1 neuron loss was most pronounced in APP23 mice. **d**: The number of neurons in the frontocentral cortex did not vary significantly among 15-18-month-old wild type, APP23, and APP48 mice. Therefore, younger animals were not studied for the number of neurons in the frontocentral cortex. *$p < 0.05$, **$p < 0.01$, ***$p < 0.001$ (Further statistical analysis: Additional file 2). Means and standard errors are depicted. (Some data were previously published in a different context [16,19]).

mice and intraneuronal Aβ in APP48 mice also contained $A\beta_{N3pE}$ and pAβ.

APP23 and APP48 mice differ considerably with respect to the mechanism of transgenic, human Aβ generation. Cleavage of Aβ from APP with the Swedish mutation as in APP23 mice occurs after APP internalization from the membrane in the early endosomal compartment [22,39]. Once generated, Aβ is rapidly secreted into the extracellular space to a large extent. In APP48 mice, on the other hand, expression of $A\beta_{42}$ with a cleaved signal sequence targets the released Aβ to the endoplasmic reticulum. Intracellular accumulation occurs in neurites and lysosomes whereas only very little $A\beta_{42}$ is secreted into the extracellular space [16]. APP48 mice lack human APP and its metabolites except for $A\beta_{42}$ whereas APP23 mice produce more $A\beta_{40}$ than $A\beta_{42}$ and, in addition to Aβ, N- and C-terminal fragments of APP. A transgenic mouse expressing only $A\beta_{40}$ with a similar construct as used in APP48 mice for $A\beta_{42}$ did not show Aβ aggregation and neuronal degeneration [16]. In double transgenic animals, expressing both $A\beta_{42}$ and $A\beta_{40}$ constructs, a similar pattern of pathological lesions was observed as in APP48 mice [16] indicating that $A\beta_{40}$ has only a marginal effect in these animals.

Both, APP23 and APP48 mice exhibited intracellular Aβ in the lysosomal compartment and in mitochondria whereas early endosomal Aβ was not seen in APP48 mice. The distribution of the transgene mRNA in the neocortex and the hippocampus as well as the expression levels were quite similar in APP23 and APP48 mice [16,20]. Accordingly, neocortical and hippocampal neurons did not vary much in the transgene expression levels in APP23 and APP48 mice. Both mouse models were used to determine the effects of Aβ under given artificial conditions. None of these two mouse models reflects human AD pathology because none showed significant neurofibrillary tangle pathology and both overexpressed a transgenic construct made to produce large amounts of Aβ [16,20].

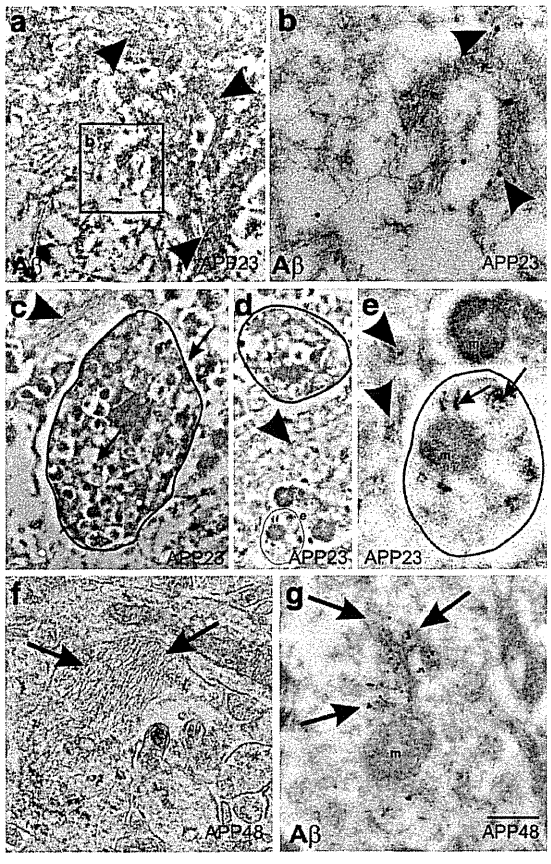

Figure 7 Electron microscopy and immunogold labeling of Aβ in APP23 and APP48 mice. a, **b**: Immunogold particles specifically labeled fibrillar Aβ (arrowheads) of a plaque in a 15-month-old APP23 mouse. At high magnification small amyloid fibrils were identified (arrowheads in **b**). They were located in the extracellular space. **c**, **d**: Dystrophic neurites (outlined structures) were associated with extracellular bundles of plaque-associated Aβ fibrils (arrowheads) in an 15-month-old APP23 mouse. Within the neurite, Aβ was localized in electron dense material near the surface as well as in the center of the neurite (arrows in **c**). **d**: A second dendrite without signs of dystrophy such as multilamellar bodies was also located near extracellular Aβ fibrils (outlined structure labeled with **e**). **e**: Higher magnification of this dendrite showed a dendrite cross section with an intact mitochondrium (m) and with condensed Aβ-positive material in the cytoplasm (arrows). Similar Aβ-positive material was found in the neighboring extracellular space (arrowhead). Both, intra- and extracellular Aβ aggregates did not exhibit fibrillar morphology. As such it is quite likely that these Aβ aggregates represent non-fibrillar oligomers and/or protofibrils occurring in the neighborhood of extracellular, plaque-associated Aβ fibrils. **f**: Fibrillar material (arrows) was observed in some dendrites of a 3-month-old APP48 mouse in an Epon-embedded, not immunostained section presumably representing the ultrastructural correlative for dendritic threads. **g**: Immunoelectron microscopy confirmed Aβ-positive material in fibrillar aggregates within dendritic threads labeled by gold particles (arrows) in APP48 mice. No Aβ was observed in the neighboring, non-altered mitochondrium (m). Calibration bar in **g** is valid for: **a** = 570 nm, **b** = 200 nm, **c** = 750 nm, **d** = 1000 nm, **e** = 275 nm, **f**, **g** = 350 nm.

Neurite and synapse degeneration in APP23 and APP48 mice

APP23 mice showed dendritic degeneration in DiI-traced commissural neurons, loss of asymmetric synapses and dystrophic neurites whereas none of these pathologies was observed in APP48 mice. In this context, it is important to note that fibrillar Aβ was present in dendrites of APP48 mice indicating that the mere presence of intracellular Aβ was not sufficient to induce this pathology. Accordingly, neuritic degeneration and loss of asymmetric synapses may either require high concentrations of extracellular $Aβ_{40/42}$ and/or the presence of APP and its metabolites including APP-derived Aβ as in APP23 mice. The amount of total $Aβ_{42}$ determined by ELISA did not explain neuritic degeneration because APP48 mice contained more $Aβ_{42}$ in the brain than 3–5 months old APP23 mice (see also [18]) although 5-month-old APP23 mice did already exhibit dendrite pathology as previously reported [18]. Consistent with our observations, the prevalence of high levels of extracellular Aβ aggregates, e.g. soluble Aβ oligomers and protofibrils and Aβ plaques have been shown to be associated with altered synapse function [40-42]. Neuritic alterations were frequently seen near amyloid plaques [43,44]. The electron microscopic detection of extracellular non-fibrillar and fibrillar Aβ-positive aggregates in association with dystrophic neurites in APP23 but not in APP48 mice further argues in favor of a critical role of extracellular Aβ in neuritic degeneration. Electrophysiological changes in response to extracellularly administered Aβ-aggregates were mainly reported for excitatory synapses [41,42]. Since asymmetric synapses represent mainly excitatory (glutamatergic) synapses [34] the loss of these synapses likely represented the result of toxic interactions with Aβ aggregates. We have detected Aβ within few dystrophic neurites in APP23 mice indicating that we cannot exclude a contribution of intraneuronal Aβ to neuritic degeneration.

The Bri-$Aβ_{42}$ mouse, that produces only extracellular $Aβ_{42}$ derived from an ABri-$Aβ_{42}$ construct did not show behavioral changes but Aβ plaques [45]. Bri-$Aβ_{40}$ mice expressing an ABri-$Aβ_{40}$ construct did not even develop plaques. These findings may argue against a contribution of extracellular Aβ to Aβ toxicity. However, it is not yet clear whether the ABri-derived $Aβ_{42}$ aggregates contain similar amounts of $Aβ_{N3pE}$ and pAβ as Aβ aggregates in APP23 or APP48 mice, whether APP expression or the presence of both, $Aβ_{42}$ and $Aβ_{40}$, is required for extracellular Aβ toxicity, or whether this mouse model did not produce enough $Aβ_{42}$ to cause symptoms.

$APP_{E693Δ}$ transgenic mice produce Aβ lacking glutamate-22 (E22Δ). This mouse model does not develop amyloid plaques but APP-derived intracellular Aβ aggregates and synapse loss [12]. Exogenous synthetic $Aβ_{E22Δ}$ also lead to synaptic alterations in hippocampal slice culture experiments or after intraventricular injection [46,47]. As

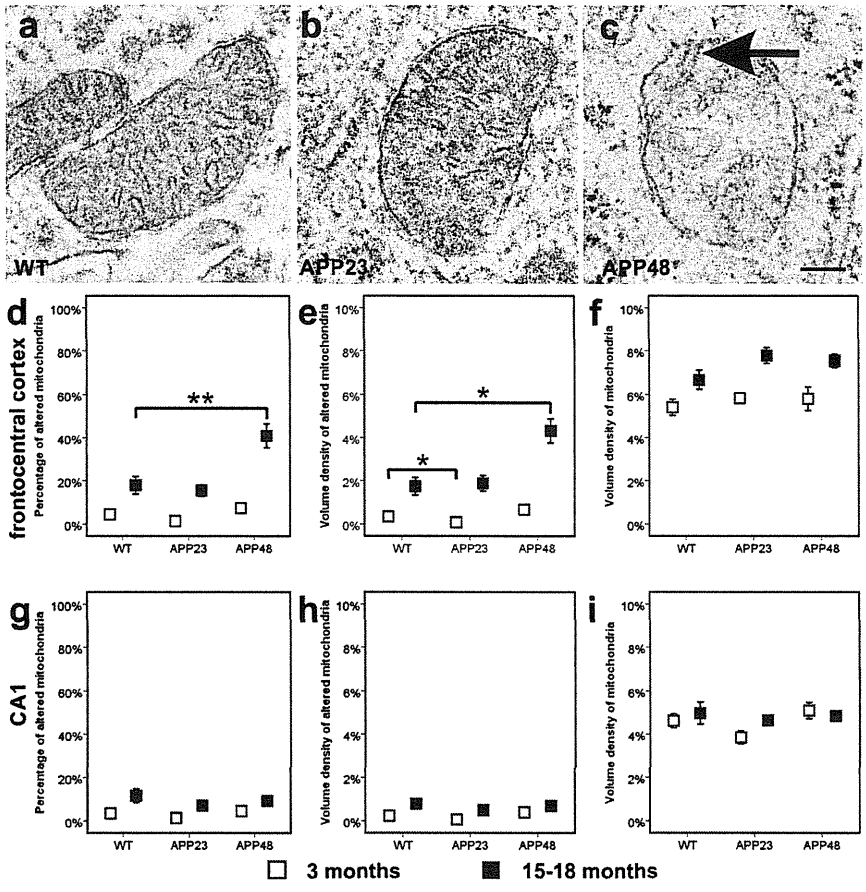

Figure 8 Electron microscopy of mitochondria in wild type, APP23, and APP48 mice. a-b: Electron microscopy showed predominantly non-altered mitochondria in nerve cell somata of wild type (WT) **(a)** and APP23 mice **(b)**. **c**: More altered mitochondria in the nerve cell somata were observed in frontocentral neurons of 18-month-old APP48 mice. Mitochondrial alteration was characterized by a loss of mitochondrial christae although the double membrane architecture and at least single christa structures (arrow) were preserved. **d-f**: The percentage of altered mitochondria in the nerve cell somata of 18-month-old APP48 mice was higher than in 15-18-month-old wild type and APP23 mice **(d)**. The volume density of altered mitochondria in the frontocentral nerve cell somata of 18-month-old APP48 mice was increased in comparison to 15-18-month-old wild type and APP23 mice **(e)**. At 3 months of age such differences in the presence of altered mitochondria were not observed. The total mitochondrial volume density, i.e. altered and non-altered mitochondria together, did not differ among the investigated mouse lines in both age groups **(f)**. **g-i**: In CA1 there were no obvious changes in the percentage and volume density of altered mitochondria in the nerve cell somata. *$p < 0.05$, **$p < 0.01$ (Further statistical analysis: Additional file 2). Means and standard errors are depicted in **d-f**. Calibration bar in **c** is valid for: **a-c** = 150 nm.

such, neuritic changes and/or synapse pathology can be explained by APP-derived Aβ production regardless of the presence of Aβ plaques whereas such changes were not reported in APP48, Bri-$Aβ_{42}$ and Bri-$Aβ_{40}$ mice, which produce non-APP derived Aβ. A further argument for a role of APP in Aβ toxicity in APP23 mice is our recent finding of a coaggregation of Aβ with C-terminal APP fragments in dispersible Aβ aggregates [19] supporting the hypothesis that APP is a molecular target of Aβ toxicity [48].

Mitochondrial alterations in APP23 and APP48 mice

APP-independent intraneuronal Aβ production and accumulation in 18-month-old APP48 mice was associated with more abundant structural mitochondrial alterations in somata of frontocentral nerve cells compared to APP23 and wild type mice. The increase of mitochondrial alterations in APP48 mice, however, was accompanied by the detection of Aβ in a moderate number of altered and non-altered neuronal somatic mitochondria whereas only few somatic mitochondria in APP23 mice exhibited Aβ and none in wild type animals. Several arguments suggest that the increase of mitochondrial alterations in APP48 mice was related to the presence of Aβ and may have functional consequences: 1) Aβ is capable of inducing apoptosis through the mitochondrial-caspase-3 pathway [49,50], 2) mitochondrial Aβ levels are associated with the extent of mitochondrial

Figure 9 Immunoelectron microscopy of mitochondria in wild type, APP23, and APP48 mice. a: Immunoelectron microscopy revealed gold-labeled Aβ (arrows) within lipofuscin-like granules in the cytoplasm of frontocentral pyramidal neurons in 15-month-old APP23 mice. **b**. Most mitochondria in the somata of frontocentral pyramidal neurons in 15-month-old APP23 mice did not contain immunogold labeled Aβ-positive material (arrowheads). **c**: Only few neuronal mitochondria exhibited single gold particles in a 15-month-old APP23 mouse indicating anti-Aβ-positive material within these mitochondria (arrow). **d**: In a few mitochondria within frontocentral pyramidal nerve cell somata of 18-month-old APP48 mice we found immunogold labeled Aβ-positive material associated with the membranes of healthy-looking mitochondria (arrow). Neighboring non-altered mitochondria often did not contain Aβ (arrowheads). Aβ fibrils were not seen inside the mitochondria. **e**: Altered mitochondria within pyramidal neurons in the frontocentral cortex of a 18-month-old APP48 mouse also exhibited single gold particles in association with their membranes indicating the presence of Aβ (arrows) although Aβ fibrils were not observed inside the mitochondria. Due to the use of LR-white embedded tissue required for post-embedding immunoelectron microscopy **(a,b)** the tissue preservation was less good than in the Epon embedded sections used for the morphological analysis of the mitochondria (Figure 8**a-c**). Calibration bar in **e** is valid for: **a, b** = 540 nm, **c** = 325 nm, **d** = 288 nm, **e** = 180 nm.

dysfunction, oxidative stress and cognitive impairment in other AD mouse models and AD [51-55], and 3) histologically altered mitochondria showed a reduced number of christa membranes presumably providing a morphological correlate for an impairment of mitochondrial function; they were found most frequently in APP48 mice which also contained more mitochondrial Aβ than APP23 mice. For APP23 mice, however, we cannot rule out that trophic effects reported for APP expression [56] compensate Aβ toxicity to mitochondria.

It is noteworthy that only mitochondria in the nerve cell somata showed increased alterations in APP48 mice whereas mitochondria in distal dendrites and axons did not exhibit differences in volume density as well as in the percentage of alterations among APP23, APP48, and wild type mice. Thus, APP-independent, intraneuronal $A\beta_{42}$ exhibited its major toxic effects on mitochondria close to its production site in APP48 mice, i.e. close to the endoplasmic reticulum. Biochemical assessment of respiratory chain complex I and complex IV, α-ketoglutarate dehydrogenase, and tricarboxylic acid cycle enzyme activity in APP48 and wild type mice did not show significant differences in forebrain homogenates (data not shown). However, the local effect in the soma is probably not sufficient to reduce the overall activities in a brain homogenate.

Two types of Aβ-induced neurodegeneration in the frontocentral cortex: somatic type and neuritic type

In the frontocentral cortex of APP23 mice neuritic degeneration and asymmetric synapse loss was found in the absence of neuron loss suggesting that both events indicate a neuritic type of nerve cell degeneration with neuritic degeneration preceding nerve cell death. APP48 mice, on the other hand, showed a different type of nerve cell damage characterized by morphologically altered mitochondria in the cell soma and thread-like Aβ aggregates in dendrites. Although the appearance of the dendrites and axons was, except for the Aβ threads, morphologically normal and no synapse loss was observed, mitochondrial changes in nerve cell somata represented early signs of a somatic type of neurodegeneration. Since mitochondrial alterations caused by Aβ have been demonstrated to induce apoptosis [49,50] it is tempting to speculate that this type of somatic neurodegeneration with increased amounts of morphologically altered mitochondria finally results in apoptosis without the development of dystrophic neurites and dendrite degeneration before cell death. Hence, APP23 mice and APP48 mice develop two different types of nerve cell degeneration in the frontocentral cortex (Figure 10): 1) APP23 mice showed a neuritic type of neurodegeneration with early neuritic and synaptic degeneration but without increased numbers of altered mitochondria; 2) APP48 mice exhibited a somatic type of neurodegeneration with increased somatic mitochondrial degeneration but morphologically intact dendrites and axons.

APP48 and APP23 mice both showed neuron loss in the CA1 region as previously described [16,17,19]. It was not accompanied by a reduction in synaptic density suggesting replacement of lost synapses by surviving neurons. Except for Aβ plaques in APP23 mice and intracellular Aβ in both transgenic animals, significant reduction of synapse densities and mitochondrial alterations could not be identified in this brain region possibly because the more vulnerable CA1 neurons die faster than altered neurons in the frontocentral cortex

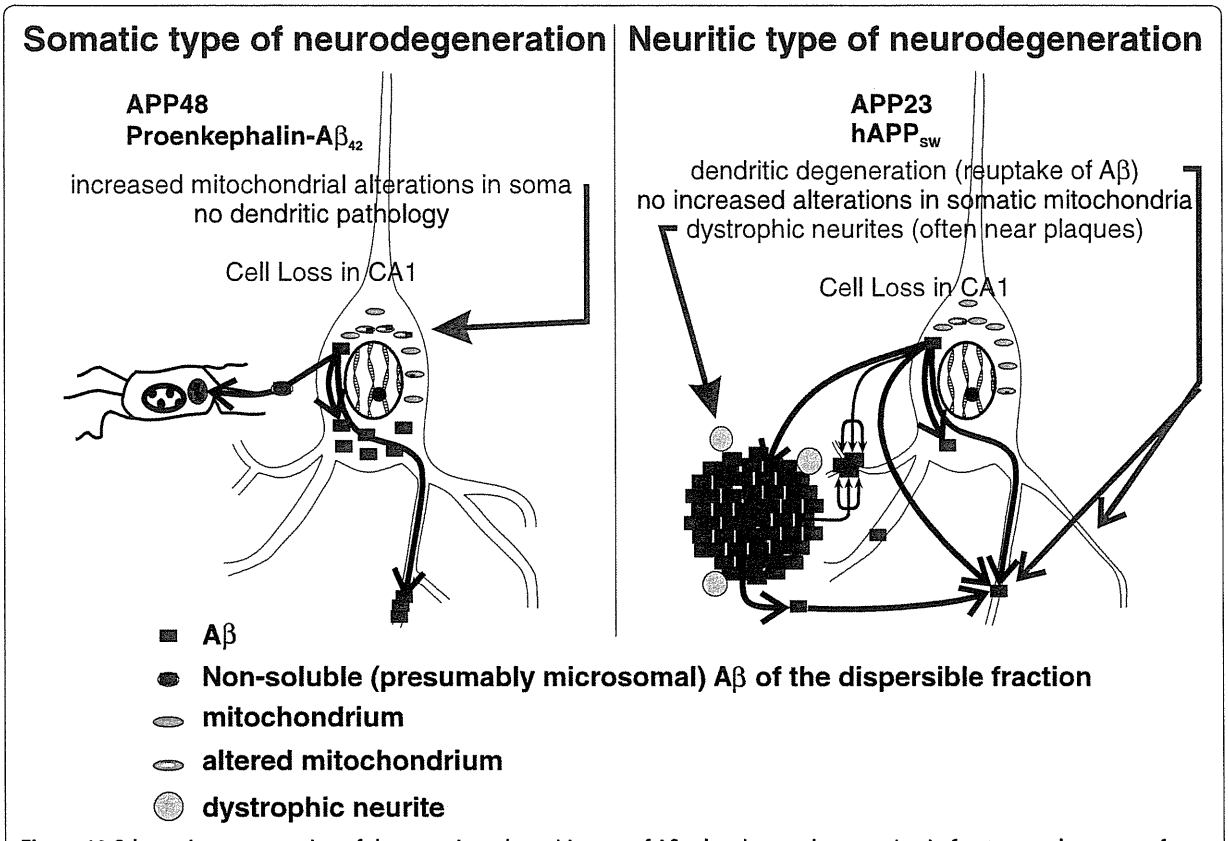

Figure 10 Schematic representation of the somatic and neuritic type of Aβ-related neurodegeneration in frontocentral neurons of APP23 and APP48 mice. In APP48 mice Aβ accumulates within neurons and in microglial cells as previously reported [16]. Extracellular Aβ is not detectable suggesting that APP-independently produced intracellular Aβ leads to functional impairment of neurons as indicated by motor deficits [16]. Mitochondrial alterations occur more frequently in the nerve cell somata of APP48 mice than in wild type and APP23 mice and are proposed to lead to apoptotic cell death as suggested previously [14] without preceding neuritic alteration. This type of somatic neurodegeneration in APP48 mice is different from that seen in APP23 mice, which contain less intracellular Aβ but significant amounts of extracellular Aβ aggregates including plaques. We propose that extra- and intracellular APP-derived Aβ causes synapse loss, dendrite degeneration and often plaque-associated, dystrophic neurites in APP23 mice indicative for a second neuritic type of neurodegeneration. Intracellular Aβ in APP23 mice may be produced within the nerve cell or may be taken up from the extracellular space [13,57-59].

and do not accumulate at early stages of nerve cell degeneration. Since 3-month-old animals have more CA1 neurons than 15-18-month-old mice (Figure 6c) and the decrease in number was higher than the age-related loss of CA1 neurons in wild type mice it appears likely that the age-related loss of CA1 neurons is enhanced by Aβ toxicity in APP23 and APP48 mice.

Although both types of Aβ-related neurodegeneration were observed in artificial mouse models that were made to produce large amounts of Aβ there are arguments for the hypothesis that both mechanisms of Aβ-related neurodegeneration are relevant in AD: 1) synapse loss and dystrophic neurites especially around neuritic plaques are well known features of AD pathology [3,60,61] that might be explained in part by the neuritic type of Aβ-related neurodegeneration and 2) mitochondrial alterations are well known in AD cases as well [54] presumably indicative for somatic type neurodegeneration in the presence of intracellular Aβ [10].

Conclusions

Our data suggest two independent mechanisms by which Aβ causes neurodegeneration (Figure 10): a neuritic type and a somatic type. The neuritic type of neurodegeneration is characterized by a loss of asymmetric synapses, degeneration of dendrites, occurrence of dystrophic neurites and is associated with the occurrence of APP-derived extra- and intracellular Aβ aggregates in APP23 mice. The somatic type of neurodegeneration shows mitochondrial alterations in the neuronal soma but no changes in neurite morphology of non-necrotic and non-apoptotic cells. It is linked to intraneuronal accumulation of APP-independently produced Aβ and functional changes in APP48 mice [16]. Both mechanisms may

finally lead to a loss of neurons as observed in the hippocampal sector CA1 in APP23 and APP48 mice [16,17]. Although these mechanisms for Aβ-related neurodegeneration have been found under artificial conditions in Aβ producing mouse models it is tempting to speculate that similar mechanisms occur in AD. APP-related production of extra- and/or intracellular Aβ, thereby, appears to be critical for neuritic and synaptic degeneration. As such, for the development of therapeutic strategies aimed at protecting neurons from AD-related degeneration it appears important to consider both types of Aβ-related neurodegeneration.

Additional files

Additional file 1: Types of commissural neurons in the frontocentral cortex as previously described [18].

Additional file 2: Statistical analysis.

Additional file 3: Western blot analysis of soluble, dispersible, membrane-associated, and insoluble (plaque-associated) Aβ in wildtype, APP48 and APP23 mice. Original blots related to Figure 3b.

Additional file 4: Mitochondrial alterations in peripheral neurites. **a-c**: Percentage of altered mitochondria (**a**), volume densities of altered mitochondria (**b**), and volume densities of all mitochondria (**c**) in peripheral neurites did not show significant changes among frontocentral neurons in wild type (WT), APP23 and APP48 mice. **d-f**: No significant differences in the percentage of altered mitochondria (**d**), volume densities of altered mitochondria (**e**), and volume densities of all mitochondria (**f**) in peripheral neurites of the CA1 sector of the Ammon's horn were found between APP48 mice and wild type controls. 3-month-old APP23 mice had less morphologically altered mitochondria (**d, e**) than wild type controls. In 15-month-old animals the trend was still visible but did not reach significance (**d, e**). *$p < 0.05$ (Further statistical analysis: *Additional file 2*).

Competing interests

D. R. Thal received consultant honorary from Simon-Kucher and Partners (Germany), and GE-Healthcare (UK).
D. Abramowski, and M. Staufenbiel are or have been employees of the Novartis Pharma AG, Basel, Switzerland.
This study was supported by DFG-grants TH624/6-1 (DRT), WA1477/6 (JW) and Alzheimer Forschung Initiative Grants #10810 (DRT) and #12854 (SK).

Authors' contributions

Neuropathology and immunohistochemistry: ARU, IK, JG, SK, HY, JW, DRT; animal breeding, genotyping and brain removal: DA, MS, DRT; Tracing and Laser Scan Microscopy: ARU, SL, DRT; Electron microscopy, immunoelectron microscopy and quantitative analyses: FS, IK, DRT; manuscript preparation: ARU, FS, MS, DRT; critical review of the manuscript: IK, DA, JG, SK, SL, HY, JW; study design, coordination and fund raising: MS, DRT. All authors read and approved the final manuscript.

Acknowledgments

The authors thank Mr. E. Schmid (Department of Electron Microscopy, University of Ulm) for help with electron microscopy and Dr. E. Capetillo-Zarate (Weill Medical College of Cornell University, New York, USA) for technical help and for reading the manuscript.

Author details

[1]Institute of Pathology - Laboratory of Neuropathology, University of Ulm, Ulm, Germany. [2]Novartis Institutes for Biomedical Research, Basel, Switzerland. [3]Department of Neurology, University of Bonn, Bonn, Germany. [4]Institute of Anatomy and Cell Biology, University of Ulm, Ulm, Germany. [5]Gunma University School of Health Sciences, Gunma, Japan.

Received: 2 November 2013 Accepted: 6 November 2013
Published: 18 November 2013

References

1. Alzheimer A: **Über eine eigenartige Erkrankung der Hirnrinde.** *Allg Zschr Psych* 1907, **64**:146–148.
2. Masters CL, Simms G, Weinman NA, Multhaup G, McDonald BL, Beyreuther K: **Amyloid plaque core protein in Alzheimer disease and Down syndrome.** *Proc Natl Acad Sci USA* 1985, **82**:4245–4249.
3. DeKosky ST, Scheff SW: **Synapse loss in frontal cortex biopsies in Alzheimer's disease: correlation with cognitive severity.** *Ann Neurol* 1990, **27**:457–464.
4. Masliah E, Terry RD, DeTeresa RM, Hansen LA: **Immunohistochemical quantification of the synapse-related protein synaptophysin in Alzheimer disease.** *Neurosci Lett* 1989, **103**:234–239.
5. Terry RD, Peck A, DeTeresa R, Schechter R, Horoupian DS: **Some morphometric aspects of the brain in senile dementia of the Alzheimer type.** *Ann Neurol* 1981, **10**:184–192.
6. Haass C, Koo EH, Mellon A, Hung AY, Selkoe DJ: **Targeting of cell-surface beta-amyloid precursor protein to lysosomes: alternative processing into amyloid-bearing fragments.** *Nature* 1992, **357**:500–503.
7. Kang J, Lemaire HG, Unterbeck A, Salbaum JM, Masters CL, Grzeschik KH, Multhaup G, Beyreuther K, Muller-Hill B: **The precursor of Alzheimer's disease amyloid A4 protein resembles a cell-surface receptor.** *Nature* 1987, **325**:733–736.
8. Hardy J, Selkoe DJ: **The amyloid hypothesis of Alzheimer's disease: progress and problems on the road to therapeutics.** *Science* 2002, **297**:353–356.
9. D'Andrea MR, Nagele RG, Wang HY, Lee DH: **Consistent immunohistochemical detection of intracellular beta-amyloid42 in pyramidal neurons of Alzheimer's disease entorhinal cortex.** *Neurosci Lett* 2002, **333**:163–166.
10. Gouras GK, Tsai J, Naslund J, Vincent B, Edgar M, Checler F, Greenfield JP, Haroutunian V, Buxbaum JD, Xu H, Greengard P, Relkin NR: **Intraneuronal Abeta42 accumulation in human brain.** *Am J Pathol* 2000, **156**:15–20.
11. Takahashi RH, Milner TA, Li F, Nam EE, Edgar MA, Yamaguchi H, Beal MF, Xu H, Greengard P, Gouras GK: **Intraneuronal Alzheimer abeta42 accumulates in multivesicular bodies and is associated with synaptic pathology.** *Am J Pathol* 2002, **161**:1869–1879.
12. Tomiyama T, Matsuyama S, Iso H, Umeda T, Takuma H, Ohnishi K, Ishibashi K, Teraoka R, Sakama N, Yamashita T, Nishitsuji K, Ito K, Shimada H, Lambert MP, Klein WL, Mori H: **A mouse model of amyloid beta oligomers: their contribution to synaptic alteration, abnormal tau phosphorylation, glial activation, and neuronal loss in vivo.** *J Neurosci* 2010, **30**:4845–4856.
13. Wirths O, Multhaup G, Czech C, Blanchard V, Moussaoui S, Tremp G, Pradier L, Beyreuther K, Bayer TA: **Intraneuronal Abeta accumulation precedes plaque formation in beta-amyloid precursor protein and presenilin-1 double-transgenic mice.** *Neurosci Lett* 2001, **306**:116–120.
14. Umeda T, Tomiyama T, Sakama N, Tanaka S, Lambert MP, Klein WL, Mori H: **Intraneuronal amyloid beta oligomers cause cell death via endoplasmic reticulum stress, endosomal/lysosomal leakage, and mitochondrial dysfunction in vivo.** *J Neurosci Res* 2011, **89**:1031–1042.
15. Tampellini D, Capetillo-Zarate E, Dumont M, Huang Z, Yu F, Lin MT, Gouras GK: **Effects of synaptic modulation on beta-amyloid, synaptophysin, and memory performance in Alzheimer's disease transgenic mice.** *J Neurosci* 2010, **30**:14299–14304.
16. Abramowski D, Rabe S, Rijal Upadhaya A, Reichwald J, Danner S, Staab D, Capetillo-Zarate E, Yamaguchi H, Saido TC, Wiederhold KH, Thal DR, Staufenbiel M: **Transgenic expression of intraneuronal Abeta42 but not Abeta40 leads to cellular Abeta lesions, degeneration and functional impairment without typical Alzheimer's disease pathology.** *J Neurosci* 2012, **32**:1273–1283.
17. Calhoun ME, Wiederhold KH, Abramowski D, Phinney AL, Probst A, Sturchler-Pierrat C, Staufenbiel M, Sommer B, Jucker M: **Neuron loss in APP transgenic mice.** *Nature* 1998, **395**:755–756.
18. Capetillo-Zarate E, Staufenbiel M, Abramowski D, Haass C, Escher A, Stadelmann C, Yamaguchi H, Wiestler OD, Thal DR: **Selective vulnerability of different types of commissural neurons for amyloid beta-protein induced neurodegeneration in APP23 mice correlates with dendritic tree morphology.** *Brain* 2006, **129**:2992–3005.
19. Rijal Upadhaya A, Capetillo-Zarate E, Kosterin I, Abramowski D, Kumar S, Yamaguchi H, Walter J, Fändrich M, Staufenbiel M, Thal DR: **Dispersible**

amyloid β-protein oligomers, protofibrils, and fibrils represent diffusible but not soluble aggregates: Their role in neurodegeneration in amyloid precursor protein (APP) transgenic mice. *Neurobiol Aging* 2012, **33**:2641–2660.

20. Sturchler-Pierrat C, Abramowski D, Duke M, Wiederhold KH, Mistl C, Rothacher S, Ledermann B, Burki K, Frey P, Paganetti PA, Waridel C, Calhoun ME, Jucker M, Probst A, Staufenbiel M, Sommer B: **Two amyloid precursor protein transgenic mouse models with Alzheimer disease-like pathology.** *Proc Natl Acad Sci USA* 1997, **94**:13287–13292.
21. Haass C, Lemere CA, Capell A, Citron M, Seubert P, Schenk D, Lannfelt L, Selkoe DJ: **The Swedish mutation causes early-onset Alzheimer's disease by beta-secretase cleavage within the secretory pathway.** *Nat Med* 1995, **1**:1291–1296.
22. Rajendran L, Honsho M, Zahn TR, Keller P, Geiger KD, Verkade P, Simons K: **Alzheimer's disease beta-amyloid peptides are released in association with exosomes.** *Proc Natl Acad Sci USA* 2006, **103**:11172–11177.
23. Galuske RA, Schlote W, Bratzke H, Singer W: **Interhemispheric asymmetries of the modular structure in human temporal cortex.** *Science* 2000, **289**:1946–1949.
24. Thal DR, Larionov S, Abramowski D, Wiederhold KH, van Dooren T, Yamaguchi H, Haass C, van Leuven F, Staufenbiel M, Capetillo-Zarate E: **Occurrence and co-localization of amyloid beta-protein and apolipoprotein E in perivascular drainage channels of wild-type and APP-transgenic mice.** *Neurobiol Aging* 2007, **28**:1221–1230.
25. Yamaguchi H, Sugihara S, Ogawa A, Saido TC, Ihara Y: **Diffuse plaques associated with astroglial amyloid beta protein, possibly showing a disappearing stage of senile plaques.** *Acta Neuropathol* 1998, **95**:217–222.
26. Saido TC, Iwatsubo T, Mann DM, Shimada H, Ihara Y, Kawashima S: **Dominant and differential deposition of distinct beta-amyloid peptide species, A beta N3(pE), in senile plaques.** *Neuron* 1995, **14**:457–466.
27. Kumar S, Rezaei-Ghaleh N, Terwel D, Thal DR, Richard M, Hoch M, Mc Donald JM, Wullner U, Glebov K, Heneka MT, Walsh DM, Zweckstetter M, Walter J: **Extracellular phosphorylation of the amyloid beta-peptide promotes formation of toxic aggregates during the pathogenesis of Alzheimer's disease.** *EMBO J* 2011, **30**:2255–2265.
28. Kumar S, Wirths O, Theil S, Gerth J, Bayer TA, Walter J: **Early intraneuronal accumulation and increased aggregation of phosphorylated Abeta in a mouse model of Alzheimer's disease.** *Acta Neuropathol* 2013, **125**:699–709.
29. Hsu SM, Raine L, Fanger H: **Use of avidin-biotin-peroxidase complex (ABC) in immunoperoxidase techniques: a comparison between ABC and unlabeled antibody (PAP) procedures.** *J Histochem Cytochem* 1981, **29**:577–580.
30. Mc Donald JM, Savva GM, Brayne C, Welzel AT, Forster G, Shankar GM, Selkoe DJ, Ince PG, Walsh DM: **The presence of sodium dodecyl sulphate-stable Abeta dimers is strongly associated with Alzheimer-type dementia.** *Brain* 2010, **133**:1328–1341.
31. Schmitz C, Hof PR: **Recommendations for straightforward and rigorous methods of counting neurons based on a computer simulation approach.** *J Chem Neuroanat* 2000, **20**:93–114.
32. DeFelipe J, Marco P, Busturia I, Merchan-Perez A: **Estimation of the number of synapses in the cerebral cortex: methodological considerations.** *Cereb Cortex* 1999, **9**:722–732.
33. Colonnier M: **Synaptic patterns on different cell types in the different laminae of the cat visual cortex. An electron microscope study.** *Brain Res* 1968, **9**:268–287.
34. Miranda R, Sebrie C, Degrouard J, Gillet B, Jaillard D, Laroche S, Vaillend C: **Reorganization of inhibitory synapses and increased PSD length of perforated excitatory synapses in hippocampal area CA1 of dystrophin-deficient mdx mice.** *Cereb Cortex* 2009, **19**:876–888.
35. Siskova Z, Mahad DJ, Pudney C, Campbell G, Cadogan M, Asuni A, O'Connor V, Perry VH: **Morphological and functional abnormalities in mitochondria associated with synaptic degeneration in prion disease.** *Am J Pathol* 2010, **177**:1411–1421.
36. Weibel ER: **Stereological principles for morphometry in electron microscopic cytology.** *Int Rev Cytol* 1969, **26**:235–302.
37. Sturchler-Pierrat C, Staufenbiel M: **Pathogenic mechanisms of Alzheimer's disease analyzed in the APP23 transgenic mouse model.** *Ann N Y Acad Sci* 2000, **920**:134–139.
38. Huang SM, Mouri A, Kokubo H, Nakajima R, Suemoto T, Higuchi M, Staufenbiel M, Noda Y, Yamaguchi H, Nabeshima T, Saido TC, Iwata N: **Neprilysin-sensitive synapse-associated amyloid-beta peptide oligomers impair neuronal plasticity and cognitive function.** *J Biol Chem* 2006, **281**:17941–17951.
39. Rajendran L, Annaert W: **Membrane trafficking pathways in Alzheimer's disease.** *Traffic* 2012, **13**:759–770.
40. Lacor PN, Buniel MC, Chang L, Fernandez SJ, Gong Y, Viola KL, Lambert MP, Velasco PT, Bigio EH, Finch CE, Krafft GA, Klein WL: **Synaptic targeting by Alzheimer's-related amyloid beta oligomers.** *J Neurosci* 2004, **24**:10191–10200.
41. Shankar GM, Li S, Mehta TH, Garcia-Munoz A, Shepardson NE, Smith I, Brett FM, Farrell MA, Rowan MJ, Lemere CA, Regan CM, Walsh DM, Sabatini BL, Selkoe DJ: **Amyloid-beta protein dimers isolated directly from Alzheimer's brains impair synaptic plasticity and memory.** *Nat Med* 2008, **14**:837–842.
42. Wang HW, Pasternak JF, Kuo H, Ristic H, Lambert MP, Chromy B, Viola KL, Klein WL, Stine WB, Krafft GA, Trommer BL: **Soluble oligomers of beta amyloid (1–42) inhibit long-term potentiation but not long-term depression in rat dentate gyrus.** *Brain Res* 2002, **924**:133–140.
43. Spires TL, Meyer-Luehmann M, Stern EA, McLean PJ, Skoch J, Nguyen PT, Bacskai BJ, Hyman BT: **Dendritic spine abnormalities in amyloid precursor protein transgenic mice demonstrated by gene transfer and intravital multiphoton microscopy.** *J Neurosci* 2005, **25**:7278–7287.
44. Tsai J, Grutzendler J, Duff K, Gan WB: **Fibrillar amyloid deposition leads to local synaptic abnormalities and breakage of neuronal branches.** *Nat Neurosci* 2004, **7**:1181–1183.
45. McGowan E, Pickford F, Kim J, Onstead L, Eriksen J, Yu C, Skipper L, Murphy MP, Beard J, Das P, Jansen K, DeLucia M, Lin W-L, Dolios G, Wang R, Eckman CB, Dickson DW, Hutton M, Hardy J, Golde T: **Aβ42 is essential for parenchymal and vascular amyloid deposition in mice.** *Neuron* 2005, **47**:191–199.
46. Takuma H, Teraoka R, Mori H, Tomiyama T: **Amyloid-beta E22Delta variant induces synaptic alteration in mouse hippocampal slices.** *Neuroreport* 2008, **19**:615–619.
47. Tomiyama T, Nagata T, Shimada H, Teraoka R, Fukushima A, Kanemitsu H, Takuma H, Kuwano R, Imagawa M, Ataka S, Wada Y, Yoshioka E, Nishizaki T, Watanabe Y, Mori H: **A new amyloid beta variant favoring oligomerization in Alzheimer's-type dementia.** *Ann Neurol* 2008, **63**:377–387.
48. Bignante EA, Heredia F, Morfini G, Lorenzo A: **Amyloid beta precursor protein as a molecular target for amyloid beta–induced neuronal degeneration in Alzheimer's disease.** *Neurobiol Aging* 2013, **34**:2525–2537.
49. Costa RO, Ferreiro E, Cardoso SM, Oliveira CR, Pereira CM: **ER stress-mediated apoptotic pathway induced by Abeta peptide requires the presence of functional mitochondria.** *J Alzheimers Dis* 2010, **20**:625–636.
50. Wang ZF, Yin J, Zhang Y, Zhu LQ, Tian Q, Wang XC, Li HL, Wang JZ: **Overexpression of tau proteins antagonizes amyloid-beta-potentiated apoptosis through mitochondria-caspase-3 pathway in N2a cells.** *J Alzheimers Dis* 2010, **20**:145–157.
51. Caspersen C, Wang N, Yao J, Sosunov A, Chen X, Lustbader JW, Xu HW, Stern D, McKhann G, Yan SD: **Mitochondrial Abeta: a potential focal point for neuronal metabolic dysfunction in Alzheimer's disease.** *FASEB J* 2005, **19**:2040–2041.
52. Dragicevic N, Mamcarz M, Zhu Y, Buzzeo R, Tan J, Arendash GW, Bradshaw PC: **Mitochondrial amyloid-beta levels are associated with the extent of mitochondrial dysfunction in different brain regions and the degree of cognitive impairment in Alzheimer's transgenic mice.** *J Alzheimers Dis* 2010, **20**(Suppl 2):S535–S550.
53. Du H, Guo L, Fang F, Chen D, Sosunov AA, McKhann GM, Yan Y, Wang C, Zhang H, Molkentin JD, Gunn-Moore FJ, Vonsattel JP, Arancio O, Chen JX, Yan SD: **Cyclophilin D deficiency attenuates mitochondrial and neuronal perturbation and ameliorates learning and memory in Alzheimer's disease.** *Nat Med* 2008, **14**:1097–1105.
54. Lustbader JW, Cirilli M, Lin C, Xu HW, Takuma K, Wang N, Caspersen C, Chen X, Pollak S, Chaney M, Trinchese F, Liu S, Gunn-Moore F, Lue LF, Walker DG, Kuppusamy P, Zewier ZL, Arancio O, Stern D, Yan SS, Wu H: **ABAD directly links Abeta to mitochondrial toxicity in Alzheimer's disease.** *Science* 2004, **304**:448–452.
55. Manczak M, Anekonda TS, Henson E, Park BS, Quinn J, Reddy PH: **Mitochondria are a direct site of A beta accumulation in Alzheimer's disease neurons: implications for free radical generation and oxidative damage in disease progression.** *Hum Mol Genet* 2006, **15**:1437–1449.
56. Mattson MP: **Cellular actions of beta-amyloid precursor protein and its soluble and fibrillogenic derivatives.** *Physiol Rev* 1997, **77**:1081–1132.
57. Ovsepian SV, Antyborzec I, O'Leary VB, Zaborszky L, Herms J, Oliver Dolly J: **Neurotrophin receptor p75 mediates the uptake of the amyloid beta**

(Abeta) peptide, guiding it to lysosomes for degradation in basal forebrain cholinergic neurons. *Brain Struct Funct* 2013. ehead of print: doi:10.1007/s00429-013-0583-x.
58. Ovsepian SV, Herms J: **Drain of the brain: low-affinity p75 neurotrophin receptor affords a molecular sink for clearance of cortical amyloid beta by the cholinergic modulator system.** *Neurobiol Aging* 2013, **34**:2517–2524.
59. Tampellini D, Magrane J, Takahashi RH, Li F, Lin MT, Almeida CG, Gouras GK: **Internalized antibodies to the Abeta domain of APP reduce neuronal Abeta and protect against synaptic alterations.** *J Biol Chem* 2007, **282**:18895–18906.
60. Dickson DW: **The pathogenesis of senile plaques.** *J Neuropathol Exp Neurol* 1997, **56**:321–339.
61. Wang D, Munoz DG: **Qualitative and quantitative differences in senile plaque dystrophic neurites of Alzheimer's disease and normal aged brain.** *J Neuropathol Exp Neurol* 1995, **54**:548–556.

doi:10.1186/2051-5960-1-77
Cite this article as: Rijal Upadhaya *et al.*: The type of Aβ-related neuronal degeneration differs between amyloid precursor protein (APP23) and amyloid β-peptide (APP48) transgenic mice. *Acta Neuropathologica Communications* 2013 1:77.

Submit your next manuscript to BioMed Central and take full advantage of:

- Convenient online submission
- Thorough peer review
- No space constraints or color figure charges
- Immediate publication on acceptance
- Inclusion in PubMed, CAS, Scopus and Google Scholar
- Research which is freely available for redistribution

Submit your manuscript at
www.biomedcentral.com/submit

BioMed Central

Eur Arch Psychiatry Clin Neurosci (2013) 263 (Suppl 2):S137–S145
DOI 10.1007/s00406-013-0449-5

ORIGINAL PAPER

Pathology of clinical and preclinical Alzheimer's disease

Dietmar Rudolf Thal · Christine von Arnim · W. Sue T. Griffin · Haruyasu Yamaguchi · Robert E. Mrak · Johannes Attems · Ajeet Rijal Upadhaya

Received: 4 September 2013 / Accepted: 16 September 2013 / Published online: 28 September 2013
© Springer-Verlag Berlin Heidelberg 2013

Abstract Alzheimer's disease (AD) is characterized neuropathologically by the presence of amyloid plaques, neuritic plaques, and neurofibrillary tangles (NFTs). These lesions occur not only in demented individuals with AD but also in non-demented persons. In non-demented individuals, amyloid and neuritic plaques are usually accompanied with NFTs and are considered to represent asymptomatic or preclinical AD (pre-AD) pathology. Here, we defined and characterized neuropathological differences between clinical AD, non-demented pre-AD, and non-AD control cases. Our results show that clinical AD may be defined as cases exhibiting late stages of NFT, amyloid, and neuritic plaque pathology. This is in contrast to the neuropathological changes characteristic of pre-AD, which display early stages of these lesions. Both AD and pre-AD cases often exhibit cerebral amyloid angiopathy (CAA) and granulovacuolar degeneration (GVD), and when they do, these AD-related pathologies were at early stages in pre-AD cases and at late stages in symptomatic AD. Importantly, NFTs, GVD, and CAA were also observed in non-AD cases, i.e., in cases without amyloid plaque pathology. Moreover, soluble and dispersible, high-molecular-weight amyloid β-protein (Aβ) aggregates detected by blue-native polyacrylamide gel electrophoresis were elevated in clinical AD compared to that in pre-AD and non-AD cases. Detection of NFTs, GVD, and CAA in cases without amyloid plaques, presently classified as non-AD, is consistent with the idea that NFTs, GVD, and CAA may precede amyloid plaque pathology and may represent a pre-amyloid plaque stage of pre-AD not yet considered in the current recommendations for the neuropathological diagnosis of AD. Our finding of early stages of AD-related NFT, amyloid, and GVD pathology provides a more clear definition of pre-AD cases that is in contrast to the changes in clinical AD, which is characterized by late stages of these AD-related pathologies. The observed elevation of soluble/dispersible Aβ aggregates from pre-AD compared to that in AD cases suggests that, in addition to more widespread AD-related pathologies, soluble/dispersible Aβ aggregates in the neuropil play a role in the conversion of pre-AD to clinical AD.

D. R. Thal (✉) · A. Rijal Upadhaya
Institute of Pathology - Laboratory of Neuropathology, Center for Biomedical Research, University of Ulm, Helmholtzstrasse 8/1, Ulm, Germany
e-mail: Dietmar.Thal@uni-ulm.de

C. von Arnim
Department of Neurology, University of Ulm, Ulm, Germany

W. S. T. Griffin
Donald W. Reynolds Center on Aging, UAMS, Little Rock, AR, USA

W. S. T. Griffin
Geriatric Research Education and Clinical Center, Veteran's Affairs Medical Center, Little Rock, AR, USA

H. Yamaguchi
Gunma University School of Health Sciences, Maebashi, Gunma, Japan

R. E. Mrak
Department of Pathology, University of Toledo, Toledo, OH, USA

J. Attems
Institute for Ageing and Health, Newcastle University, Newcastle upon Tyne, UK

Keywords Alzheimer's disease · Amyloid · Neurofibrillary tangles · Clinical stage

Introduction

Alzheimer's disease (AD) is histopathologically characterized by amyloid plaques, neurofibrillary tangles (NFTs), neuropil threads, and neuritic plaques [20]. Cerebral amyloid angiopathy (CAA) and granulovacuolar degeneration (GVD) are further pathological changes associated with AD [22, 36, 40, 41, 47]. Amyloid plaques and CAA lesions consist of aggregates of the amyloid β-protein (Aβ) [16, 29]. In addition to amyloid plaques and CAA, soluble and dispersible Aβ can be found in brain homogenates [24, 26, 34, 35, 38]. NFTs and neuropil threads contain aggregated abnormal phosphorylated τ-protein [6, 18]. Neuritic plaques are amyloid plaques, which are associated with dystrophic neurites [13, 44]. GVD represents granules in the neuronal cytoplasm, which consist of abnormal phosphorylated τ-protein, phosphorylated transactive response DNA-binding protein TDP-43, casein kinases, and other proteins [14, 15, 19, 23, 37, 49]. All of these lesions are found not only in demented individuals with symptomatic AD but also in non-demented persons [3, 8, 33, 40, 41, 43].

The current National Institute of Aging–Alzheimer Association (NIA-AA) neuropathological consensus guidelines for the diagnosis of AD recommend reporting levels of AD pathology in the brain regardless of the clinical status of a given individual. AD pathology is considered whenever Aβ plaques are observed [20]. Although the clinical diagnosis of AD is restricted to demented individuals [30], it has been proposed to categorize non-demented patients who exhibit AD-related biomarker profiles as preclinical AD (pre-AD) [39]. Thus, the neuropathological identification of AD pathology in non-demented individuals serves as a biomarker for AD, and those non-demented individuals who have such AD pathology can be classified as pre-AD cases. The NIA-AA guidelines for the neuropathological diagnosis of AD define AD through the presence of Aβ plaques [20]. In an analogous fashion, pre-AD cases at the neuropathological level may be defined as non-demented cases with Aβ plaques and non-AD cases as those non-demented individuals who do not have Aβ plaques. The presence or absence of NFT pathology, which can also occur in non-AD tauopathies, is not considered in this classification [20].

Here, we studied 766 autopsy brains for AD-related lesions correlated this with the presence or absence of dementia. Based on this, these cases were classified as symptomatic AD, pre-AD, or non-AD controls.

Materials and methods

Neuropathology

A total 766 autopsy cases were studied (Tables 1, 2). At the time of autopsy, brains were fixed in a 4 % aqueous solution of formaldehyde. Following fixation, the medial temporal lobe (MTL) and tissue from the occipital cortex containing the primary visual field were embedded in paraffin. Paraffin sections were cut at 12 μm thickness. Histopathological diagnoses of AD were made based on the analysis of sections of MTL and occipital cortex stained with the Gallyas and Campbell-Switzer silver techniques, and/or on sections immunoreacted with anti-abnormal τ-protein (anti-PHF-τ; AT-8; Innogenetics, Belgium, 1/1000) and anti-$A\beta_{17-24}$ (4G8; 1/5000, formic acid pretreatment, Sigma-Aldrich, St. Louis, USA). NFT staging and the assignment of Consortium to Establish a Registry for Alzheimer's Disease (CERAD) scores for neuritic plaque density were performed on Gallyas-stained and/or anti-PHF-τ-immunoreacted sections [1, 7, 8, 31]. The distribution of amyloid plaques in the MTL (Aβ phase (MTL)) was assessed according to previously published criteria [44]. Basically, the distribution of Aβ plaques was assessed semiquantitatively to determine the severity of Aβ plaque pathology [43]. Aβ phase (MTL), Braak-NFT stages, and CERAD scores for neuritic plaques were used to determine the degree of AD pathology according to the NIA-AA guidelines [20]. CAA was detected by anti-$A\beta_{17-24}$ immunoreactions and staged in 207 cases according to the following previously published scheme [41]: neocortical CAA (stage 1), additional allocortical and cerebellar CAA (stage 2), and subcortical CAA (brain stem, basal ganglia) (stage 3). GVD was observed in 161 cases using anti-pTDP43 immunostaining (pS409/410-2, Cosmo Bio Co., Ltd, Tokyo, Japan, 1/10,000, microwave pretreatment) and staged according to published criteria [40]: Stage 1 represents GVD restricted to the CA1 region in the Ammon's horn, stage 2 shows additional GVD in CA4 and/or the entorhinal region, stage 3 shows extension into the temporal neocortex, stage 4 to the amygdala and/or the hypothalamus, and finally, stage 5 GVD also involves midbrain nuclei, the cingulate gyrus, and/or frontal cortex. For CAA and GVD staging, additional paraffin sections of the superior frontal gyrus, cingulate gyrus, amygdala, basal ganglia, hypothalamus, midbrain, and/or pons were immunostained for Aβ or pTDP43. These additional sections were analyzed in those cases in which CAA or GVD was observed in MTL and occipital lobe sections.

Clinical dementia rating (CDR) scores were retrospectively obtained in 282 cases by screening the clinical records as reported previously [43]. Cases with CDR scores of 0.5 and higher were considered demented or cognitively impaired. In

Table 1 Description of the case collective

	N	Mean age in years (range)	Male/ female	Mean Aβ phase-MTL (range)	Mean NFT stage (range)	Mean CERAD score (range)
All cases	766	74.75 (20–104)	420/346	1.81 (0–4)	2.3 (0–6)	0.77 (0–3)
AD	114	81.52 (56–101)	44/70	3.74 (1–4)	4.96 (3–6)	2.44 (0–3)
Pre-AD	404	75.98 (48–104)	230/174	2.38 (1–4)	2.15 (0–6)	0.54 (0–3)
Non-AD	248	69.64 (20–98)	146/102	0 (0)	1.31 (0–4)	0 (0)

Entire sample subclassified into AD, pre-AD, and non-AD cases

Table 2 List of cases used for biochemical analysis

Case no.	Diagnosis	Age	Gender	Aβ phase (MTL)	Braak-NFT-stage	CERAD-plaque-score
1	no AD	60	M	0	0	0
2	no AD	66	M	0	1	0
3	no AD	69	F	0	1	0
4	no AD	71	F	0	1	0
5	pre-AD	73	F	3	1	0
6	pre-AD	84	F	3	2	0
7	pre-AD	71	M	3	2	1
8	pre-AD	77	F	3	2	0
9	pre-AD	78	F	3	2	0
10	AD	79	F	3	4	2
11	AD	78	M	4	4	1
12	AD	62	F	4	6	3
13	AD	91	F	3	4	1
14	AD	84	M	4	6	3
15	AD	64	F	4	6	3

Control and AD cases not included in Fig. 2 were previously included in a study where these results are depicted [35]

M male, *F* female

484 cases, the clinical records provided information about the presence or absence of dementia according to DSM-IV but did not provide sufficient information to determine the CDR score. Demented cases with AD pathology according to recommended criteria for the neuropathological diagnosis of AD [20] and lacking evidence of other forms of dementia were classified as clinical AD cases. When applying the NIA-AA criteria, controls were defined by the absence of any Aβ plaques. Non-demented cases with Aβ plaques were neuropathologically categorized as pre-AD cases.

All autopsy brains were collected from individuals who died in university or municipal hospitals in Germany (Bonn, Frankfurt/Main, Mainz, Offenbach/Main, Ulm), USA (Little Rock, AR), the United Kingdom (Newcastle upon Tyne), or Austria (Vienna) in accordance with local ethical committee guidelines and the laws governing the use of human tissue.

Biochemical analysis

To characterize the role of soluble/dispersible Aβ in the course of clinical and preclinical AD, fresh-frozen human brain tissue from 6 AD, 5 pre-AD, and 4 control cases obtained at autopsy was used for the determination of native Aβ aggregates in the AD and control brain (Tables 1, 2).

Protein extraction from fresh-frozen human occipital (Brodmann areas 17, 18, 19) and temporal cortex (Brodmann areas 35 and 36) was carried out in 2 ml of a 0.32 M sucrose solution with protease and phosphatase inhibitor cocktail (PhosSTOP, Roche, Mannheim, Germany). The tissue was homogenized as previously described [34]. The homogenate was kept on ice for 30 min and the supernatant was clarified by centrifugation for 30 min at 14,000*g*. To avoid separation of high-molecular-weight proteins into the membrane-associated and plaque-associated fractions, centrifugation speeds higher than 14,000*g* were not used. The resultant supernatant, containing soluble and dispersed proteins as previously shown [34], was aliquoted into an appropriate volume and stored at −80 °C until used. Protein amounts were determined using a BCA Protein Assay (Bio-Rad, Hercules, CA, USA).

For BN-PAGE of the supernatant containing soluble and dispersed proteins, 50 μg of total protein was prepared with 4X NativePAGE sample buffer (Invitrogen) and subjected to native PAGE 4–16 % Bis–Tris gel electrophoresis according to the manufacturer's protocol (Invitrogen). Native-Mark unstained protein standards (Invitrogen) were used as molecular weight markers. The gel was equilibrated in transfer buffer containing 0.2 % SDS for 10 min. After protein transfer onto nitrocellulose membranes (Bio-Rad), the membranes were boiled in PBS buffer in a microwave oven for 6 min followed by blocking with non-fat dry milk (Roth, Karlsruhe, Germany) for 1 h at room temperature.

For immunodetection of the blotted proteins, the membranes were incubated 24 h at 4 °C with the anti-$A\beta_{42}$ antibody MBC42 (1/500 [48]). This antibody was used because we have previously shown that it detects $A\beta_{42}$ in BN-PAGE protein analysis without cross-reaction with amyloid precursor protein (APP) [35]. Since soluble/dispersible $A\beta_{40}$ could not be detected in an earlier study after

BN-PAGE analysis of AD brain homogenates [35], we focused in the present study on $A\beta_{42}$ aggregates. After rinsing steps, the corresponding secondary antibodies were applied for 2 h at RT. Blots were developed with an ECL detection system (Supersignal Pico Western system, ThermoScientific-Pierce, Waltham, MA, USA) and illuminated in ECL Hyperfilm (GE Healthcare, Buckinghamshire, UK).

Statistical analysis

Comparisons between non-AD, pre-AD, and AD cases were assessed for statistical significance using the Mann–Whitney U test. p values were corrected for multiple testing. SPSS Statistics 19 software (SPSS, Chicago, IL, USA) was used to perform the statistical analysis.

Results

Distribution of Aβ plaques, NFTs, neuritic plaques, CAA, and GVD in clinical AD, pre-AD, and non-AD control cases

Mean ages, Aβ phases, NFT stages, and CERAD scores of AD, pre-AD, and non-AD cases are provided in Table 1. AD cases in general had more widely distributed Aβ plaques, NFTs, neuritic plaques, CAA, and GVD—as represented by the respective phases, stages, and scores—than did pre-AD or control cases ($p < 0.002$). Non-AD cases did not exhibit Aβ plaques and neuritic plaques but some cases did show early stages of NFT and GVD pathology.

In detail, Aβ plaques were not found, by definition, in non-AD cases. In pre-AD cases, Aβ phases (MTL) 1–3 were predominantly found, whereas nearly all AD cases had Aβ phase (MTL) 4, i.e., end-stage Aβ pathology (Fig. 1a). Thus, the distribution of Aβ plaques as represented by phases of Aβ deposition in the MTL [44] was higher in AD than in pre-AD cases ($p < 0.002$). The Aβ pathology in pre-AD cases was also more severe than that in non-AD controls ($p < 0.002$) inasmuch as, by definition, all pre-AD and AD cases had Aβ plaques and non-AD did not.

The distribution of NFTs as represented by NFT stage [8] was higher in AD than in pre-AD cases ($p < 0.002$; Fig. 1b). Similarly, pre-AD cases exhibited more widely distributed NFT pathology than did non-AD cases ($p < 0.002$). However, most non-AD cases exhibited early NFT stages, indicating that there are a significant number of cases without Aβ plaques, classified as non-AD, that already have NFT pathology. All AD cases, 95.4 % of the

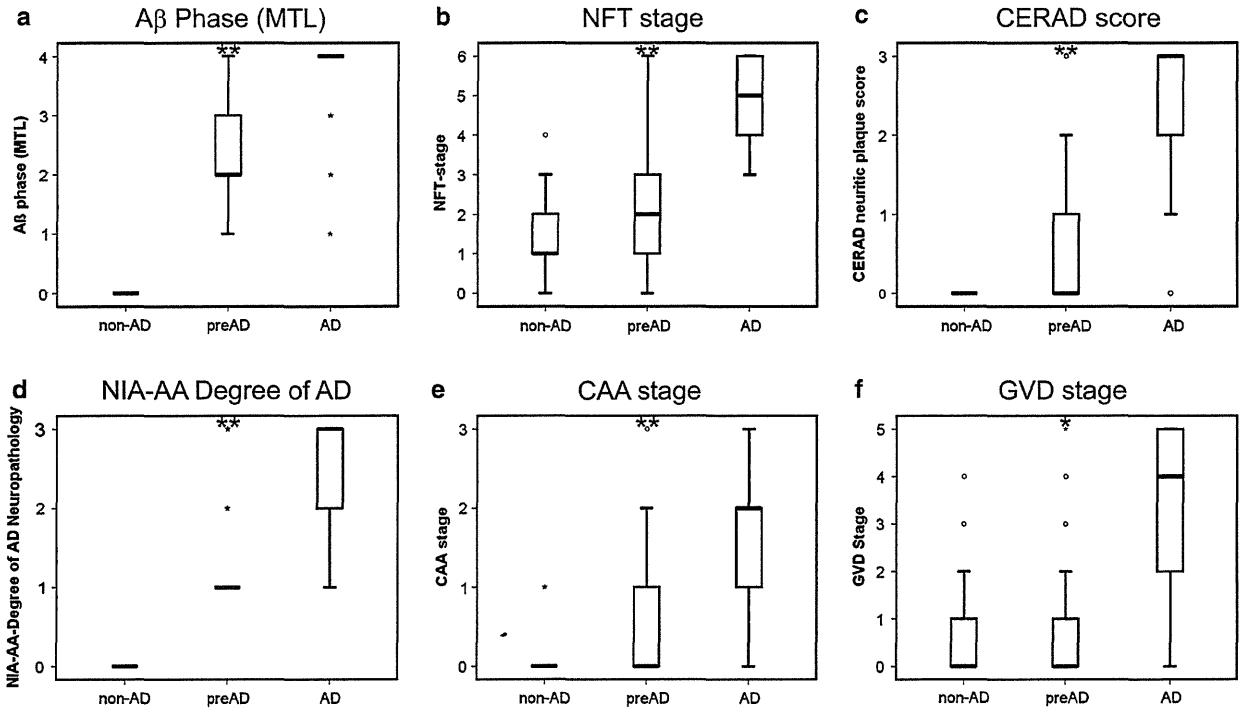

Fig. 1 Box plot diagrams indicating the distribution of Aβ phases within the MTL (**a**), NFT stages (**b**), CERAD scores for neuritic plaque pathology (**c**), NIA-AA degrees of AD pathology (**d**), CAA stages (**e**), and GVD stages (**f**) for clinical (AD) and preclinical (pre-AD) AD cases and for controls with no AD, according to the current guidelines for clinical and neuropathological diagnosis of AD [20, 30, 39]. Mann–Whitney U test corrected for multiple testing: $*p < 0.05$, $**p < 0.01$